Geofísica Internacional (2025) **64-1**: 1455 - 1477

The Chuquibamba Landslide Western Cordillera, Peru revisited: New evidence of a dry debris avalanche

Sánchez-Núñez, J.M.*[1], Macías, J.L.[2], Arce, J.L.[3] and Gómez, J.C.[4]

Abstract

Landslides represent a serious mountain hazard to lives and infrastructure, especially when geological factors such as highly fractured rocks, faulting, steep topography, and weathering combine with seismic triggering factors. Considering the potential of producing outcomes, we study the Chuquibamba rotational landslide that runs along the NW-SE Incapuquio-Challaviento fault system in southernmost Peru. Its elongated U-shaped and polylobate crown scarp is typical of fault-related landslides, and it is carved into the ignimbrites of the Chuquibamba Formation. The geomorphology of the failure and its associated deposit define seventeen coalescing rotational slides and a widespread debris avalanche. This deposit, the main topic of this study, dated at ca. 102 ± 5 ka using ^{10}Be (from previous works), is confined to the lower parts of the Grande River valley. It is exposed for about 22.5 km from 3,900 to 1,167 masl with its main front located at ~ 10 km upstream of the Majes River. It covers an area of 33.64 km^2 with a minimum volume of 0.72 km^3. The resulting deposit has an H/L = 0.12, which is typical of dry debris avalanches elsewhere. It consists of block and matrix facies that have different textural and granulometric features. At the time of its emplacement, the moving avalanche overpassed 20 and 12 m-high obstacles, attaining minimum speeds of 20 and 15 m/s at distances of 15 and 20 km from the source, respectively. After the landslide emplacement, the debris avalanche was re-mobilized by intense rains that produced debris flows, as attested by outcrops along the extension of the debris avalanche and beyond its front. All the features of the Chuquibamba dry avalanche, along with modern seismicity and the intersection of active faults in the region, suggest that the failure had a tectonic origin (uplift and movement along faults) instead of deglaciation, extraordinary rain, or extreme rock weathering. Therefore, landslide generation is a potential hazard in this area of Peru.

Key words: Rotational landslide, debris avalanche, facies, Chuquibamba, Peru.

Resumen

Los deslizamientos en zonas montañosas representan un serio peligro para la vida e infraestuctura, en particular cuando se combinan factores geológicos con factores sísmicos que los pueden detonar. Considerando la posibilidad de generación de estos procesos, estudiamos el caso del deslizamiento rotacional de Chuqibamba, que se alinea a lo largo del sistema de fallas NW-SE Incapuquio-Challaviento en el extremo sur del Perú. La forma elongada en "U" del deslizamiento y su corona de escarpe poli-lobulada, son rasgos típicos de deslizamientos relacionados con fallas que afectaron hasta las ignimbritas de la Formación Chuquibamba. La geomorfología del colapso y depósitos asociados, definen diecisiete bloques rotacionales coaslescentes y un depósito extenso de avalancha de escombros. Este depósito, objeto de este estudio, fechado en aproximadamente 102 ± 5 ka por ^{10}Be (tomado de trabajos previos), está confinado en el valle del Río Grande. Aflora a lo largo de 22.5 km, desde los 3,900 hasta 1,167 msnm con el frente principal ubicado a ~10 km río arriba del Río Majes. El depósito cubre un área de 33.64 km^2, un volumen mínimo de 0.72 km^3 con un H/L = 0.12, típico de flujos de escombros secos. La avalancha superó obstáculos de 20 y 12 m de altura, con velocidades mínimas de 20 y 15 m/s a distancias de 15 y 20 km desde la fuente respectivamente. Después del emplazamiento del colapso, la avalancha de escombros fue removilizada por lluvias intensas produciendo flujos de escombros, tal como quedó registrado en los afloramientos en todo el depósito y más allá de éste. Todas las características de la avalancha seca de Chuquibamba, junto con la sismicidad moderna de la región, sugieren que el colapso tuvo un origen tectónico (levantamiento y movimiento a lo largo de fallas), más que deglaciación, lluvias extraordinarias o intemperismo severo de las rocas. Por lo tanto, la generación de deslizamientos es un peligro potencial en esta zona del Perú.

Palabras clave: Deslizamiento rotacional, avalancha de escombros, facies, Chuquibamba, Perú.

Received: June 18, 2024; Accepted: December 6, 2024; Published on-line: January 1, 2025.

Editorial responsibility: Dra. Lucía Capra Pedol

* Corresponding author: Juan Manuel Sánchez-Núñez, sanchez0120@gmail.com
[1] Centro Interdisciplinario de Investigaciones y Estudios sobre Medio Ambiente y Desarrollo (CIIEMAD), IPN, 30 de Junio de 1520 s/n, La Laguna Ticoman, Gustavo A. Madero, 07340 Ciudad de México, México.
[2] Instituto de Geofísica, Universidad Nacional Autónoma de México, Cd. De México, Coyoacán, 04510, México, jlmacias@igeofisica.unam.mx
[3] Instituto de Geología, Universidad Nacional Autónoma de México, Cd. De México, Coyoacán, 04510, México, jlarce@geologia.unam.mx
[4] Instituto Geofísico del Perú, Calatrava 216, La Molina, Lima 12, Perú, jgomez@geo.igp.gob.pe

José Luis Arce-Saldaña, Juan Manuel Sánchez-Núñez, José Luis Macías Vázquez, Juan Carlos Gómez

https://doi.org/10.22201/igeof.2954436xe.2025.64.1.1810

1. Introduction

The Andes is a region in which a large number and variety of historical landslides have occurred (Nadim *et al.*, 2006; PMA, 2007; PMA, 2008; Mergili *et al.*, 2014; Delgado *et al.*, 2020). Mergili *et al.* (2014) reported 104 landslides that were classified as disasters in the Andean countries (Argentina, Bolivia, Chile, Colombia, Ecuador, Peru, and Venezuela) between 1901 and 2011. Eight landslides occurred between 1971 and 1999 and killed at least 65,790 people in those countries (Mergili *et al.*, 2014). Out of those eight events, Peru has suffered disproportionally, with four landslides resulting in the loss of 12,250 lives. Moreover, during the last forty years, landslides and flooding in Peru have increased due to climate change alongside heavy precipitation and peak glacier runoff (Brügger *et al.*, 2021).

Debris avalanches are catastrophic landslides that transport masses with volumes between 10^7 and 10^{11} m^3. These landslides are considered to be one of the most destructive processes in nature (e.g., Mehl and Schmincke, 1999; Dufresne *et al.*, 2010; Godoy *et al.*, 2012; Cui *et al.*, 2022). The moving avalanche mass may reach speeds between 50 and 150 m/s, thus turning them into extremely dangerous phenomena for both infrastructure and human lives (Bowman *et al.*, 2012; Wang *et al.*, 2015). Debris avalanches may be triggered by different factors such as seismic, volcanic, and extreme hydrometeorological events, and they may be enhanced by local factors such as weathered/fracturing rocks, steep topography, faulting, and anthropogenic activity (Korup *et al.*, 2007; Dufresne *et al.*, 2016; Wang *et al.*, 2015, 2017).

Delgado *et al.* (2022) built up a landslide inventory along the northernmost Central Western Andes (ca. 15° - 20°S); they compiled a landslide database (typology, size, abundance, and relation to geologic, tectonic, and climatic settings) with statistical analysis to gain insights into their controlling factors. They found that most of them are paleo landslides dominated by rockslides (86%) and rock-avalanche types (14%). These events have been common in the past and represent excellent examples of debris avalanches and debris flows worldwide for which detailed studies are important to understand their origins, flow behaviors, and deposit characteristics. In this study, we focus on the ancient Chuquibamba debris avalanche deposit, which is exposed along the Grande River valley, in the Province of Condesuyos, Department of Arequipa. Its name is inspired by the nearby village that sits in the middle of the valley.

Previous works have described the deposit as a 40 km^3 mega debris flow of ~102 ± 5 ka in age (Margirier *et al.*, 2015) with 30 km of runout down the valley. More recently, Thouret *et al.* (2017) described it as a rotational landslide produced by retrogressive failures that generated at least four debris avalanche deposits with different stages of erosional amphitheater dated between 120-40 ka. Based on morphology, field descriptions, and sedimentological analysis, we re-examine this deposit and we provide new light on the origin of the landslide that modified the morphology of the valley, creating a large U-shaped landslide scar and originating a dry debris avalanche deposit. The event was most likely triggered by an earthquake. In this study, we present the distribution, stratigraphic columns, and field observations of the deposit. In addition, we discuss the granulometric characteristics of the deposit and propose an alternative explanation of its genesis.

1.1 Terminology

The term *landslide* is used in this paper to describe a downward and outward movement of a slope under the influence of gravity, and it implies mass transport as a process that does not require a transporting medium such as water, ice, or air (Cruden and Varnes, 1996). The term *complex landslide* is used to describe two or more types of mass movements, occurring where the initial failure type transitions into another as it moves downslope (Huggett, 2017; Dikau *et al.*, 1996a, 1996b). A *debris avalanche* moves as a mass of rock, soil, and snow that occurs when a flank of a mountain collapses and slides downslope; they move at a very high speeds and may travel several kilometers before coming to rest (Dikau *et al.*, 1996a; Strom *et al.*, 2019). The term *hummock* is a topographic feature of large landslides and rockslide-debris avalanches that is common in both volcanic and non-volcanic settings (Paguican *et al.*, 2011; 2014). It can be a rounded or conical knoll, mound, hillock, or other small elevation change, generally of equidimensional shape, and not ridge-like. The term *megablock* (>100 m in diameter; Mehl and Schmincke, 1999) is used to refer to a rock produced by fragmentation on a very large scale which contains debris avalanche blocks (0.25-100 m) that are shattered but only slightly rotated (Siebert, 2002; Crosta *et al.*, 2007; Sturm *et al.*, 2015). The term *matrix* is used for fragments < 2 mm (fine sand, silt, and clay). The matrix can be part of the total deposit, or it may constitute the intraclast material when the blocks (or megablocks) are entirely shattered (Crosta *et al.*, 2007).

2. Methods

The research was conducted in three stages. First, we collected the relevant geographical and geological data from the literature. The geographic and geologic data of the Chuquibamba area were collected and analyzed in a spatial database. To produce the Digital Elevation Model (DEM), we interpreted 15 m contour lines from INGEMMET (Instituto Geológico, Minero y Metalúrgico), Peru, and 12.5 m contour lines provided by the Alaska Satellite Facility (ASF) (UAF-NASA). We used the Digital Model of

Terrain (DMT) to prepare DEM-derived images (hill shade, hypsometric, slope, and anaglyphs). Morphological analysis of the area was carried out on Landsat TM8 (path = 4, row = 71) with Operational Land Imager (OLI) sensor, at a 30 m resolution, panchromatic images (at 15 m resolution), and high-resolution multispectral images. We used the ArcGIS Base Map, the Google Earth imagery server, and vectorial cartography (e.g., drainage pattern, urban infrastructure, roads, and towns). The geological information was derived from Thouret *et al.* (2007, 2016), Zavala (2017), and Schildgen *et al.* (2010), and the cartographic information was taken from Olchauski and Dávila (1994). All these geological and morphological data from previous works were compiled using ERDAS 9.1 and ArcGis 10.4 commercial software to produce a preliminary geologic map which was then modified during fieldwork to generate the final map.

To define the volume of the Chuquibamba debris-avalanche deposit, the topographic difference method was used. This method works by calculating the volumetric surface difference between two models stored as a terrain data set in the form of triangulated irregular networks (TIN). First, a 12.5 m pixel resolution DEM and the 3D Analyst module of a Geographic Information System (ArcGis) were used. We then calculated the approximate volume between the elevations at the base surface (z-base) and the top of the analyzed area (z-top).

The second stage incorporated the fieldwork performed in 2011 and 2012. This work involved drawing 28 stratigraphic sections of the area, which were then used to characterize the deposits and correlate outcrops.

In the third stage of the investigation, we carried out the sedimentological study of the deposit by describing the 28 outcrops; we took 84 standardized photographs and collected 28 samples, one for each site. In total, we used three methodologies for this study: i) Rosiwal intersections (e.g., Chayes, 1956)—this technique was used for inaccessible areas and large fragments. An optical image (photographic) analysis of each outcrop was performed to quantify components greater than -6Φ; ii) Analysis by sieving—we collected 28 sediment samples (~ 3 kg per sample), which were dried in an oven at 70°C for 24 hours. The samples were processed with sieves at intervals of 1Φ from -6Φ to 4Φ; iii) Scanning by laser diffraction, where the measurement of fine particles (> 4Φ) was carried out under the physical principle described by Stokes' Law. We integrated the results of the three techniques to obtain the total particle size spectrum, generating frequency histograms and cumulative curves for each sample. To get the statistical parameters, we used the GRADISTAT program, while considering the criteria of Inman (1952) and Folk (1974). We carried out these activities in the Particle Analysis and Mineral Separation Laboratory of the Geophysics Institute, Morelia, Michoacan, Mexico.

3. Tectonic overview

The Chuquibamba landslide is situated in the Western Cordillera Domain (WCD), southern Central Andes (Roperch *et al.*, 2006). The area is controlled by the subduction of the Nazca plate beneath the South American plate at the South American trench (Figure 1A). From a geologic point of view, the Western Cordillera began its formation during the Late Cretaceous when the coastal domain began to rise and overthrust toward the east (Pfiffner and Gonzalez., 2013; Armijo *et al.*, 2015; Freymuth *et al.*, 2015). Magmatic activity occurs mainly in the southwestern region of the Chuquibamba quadrangle during the Cretaceous and Late Cretaceous-Paleogene. These intrusions emplaced granodiorites and tonalites, which formed the prolongation of the Batholith of the coast outcrops (Olchauski and Dávila, 1994; Thouret *et al.*, 2016).

During the Neogene and Quaternary, explosive volcanism dispersed voluminous ignimbrites that are the main characteristic of the Andean Central Volcanic Zone (Thouret *et al.*, 2016). In southern Peru, this volcanism emplaced the second-largest sheets of the ignimbrite field, covering at least 25,000 km^2. Among these rocks are the ignimbrites of the Camaná-Majes-Colca area, which are well-exposed in the altiplano. The town of Chuquibamba sits atop all of these sequences. The Río Colca region includes 42 ignimbrites and 22 lava flows, which date from the Late Miocene to the Quaternary (Thouret *et al.*, 2007, 2016),

The Chuquibamba area is a region with strong regional structural controls (Figure 1). It is transected by the sinistral transcurrent Incapuquio Fault System, known as Incapuquio-Challaviento, and the Incapuquio-Micalaco-Capillune fault systems in the Tacna and Moquegua departments, respectively (Jacay *et al.*, 2002; Gunnell *et al.*, 2010; Thouret *et al.*, 2016; Benavente *et al.*, 2017). Benavente *et al.* (2017) presented a detailed structural map in addition to the neotectonic, seismic risk, and the Arequipa relief evolution that included the region of Chuquibamba (Figure 1B). In their structural map they described all the main fault zones of the Incapuquio Fault System, including several active faults.

The fault system facilitated the Late Cretaceous – Early Paleogene magmatism and formed the active border of the Moquegua basin during the Oligocene (Thouret *et al.*, 2016, 2017). The Incapuquio Fault System is still active, as attested by present-day earthquakes (Jacay *et al.*, 2002; Benavente *et al.*, 2017). The National Civil Defense Institute and the Geophysical Institute of Peru (IGP) have reported at least 85 earthquakes with magnitudes > 6 in the Western Cordillera of the Andes (from 1890 to 2001). During the last 200 years, the IGP has recorded at least eight earthquakes in the Chuquibamba-Cotahuasi Quadrangles (Arequipa area) occurring in 1821, 1868, 1913, 1942, 1958, 1960, 2001, and 2005 (**Appendix 1**). These earthquakes

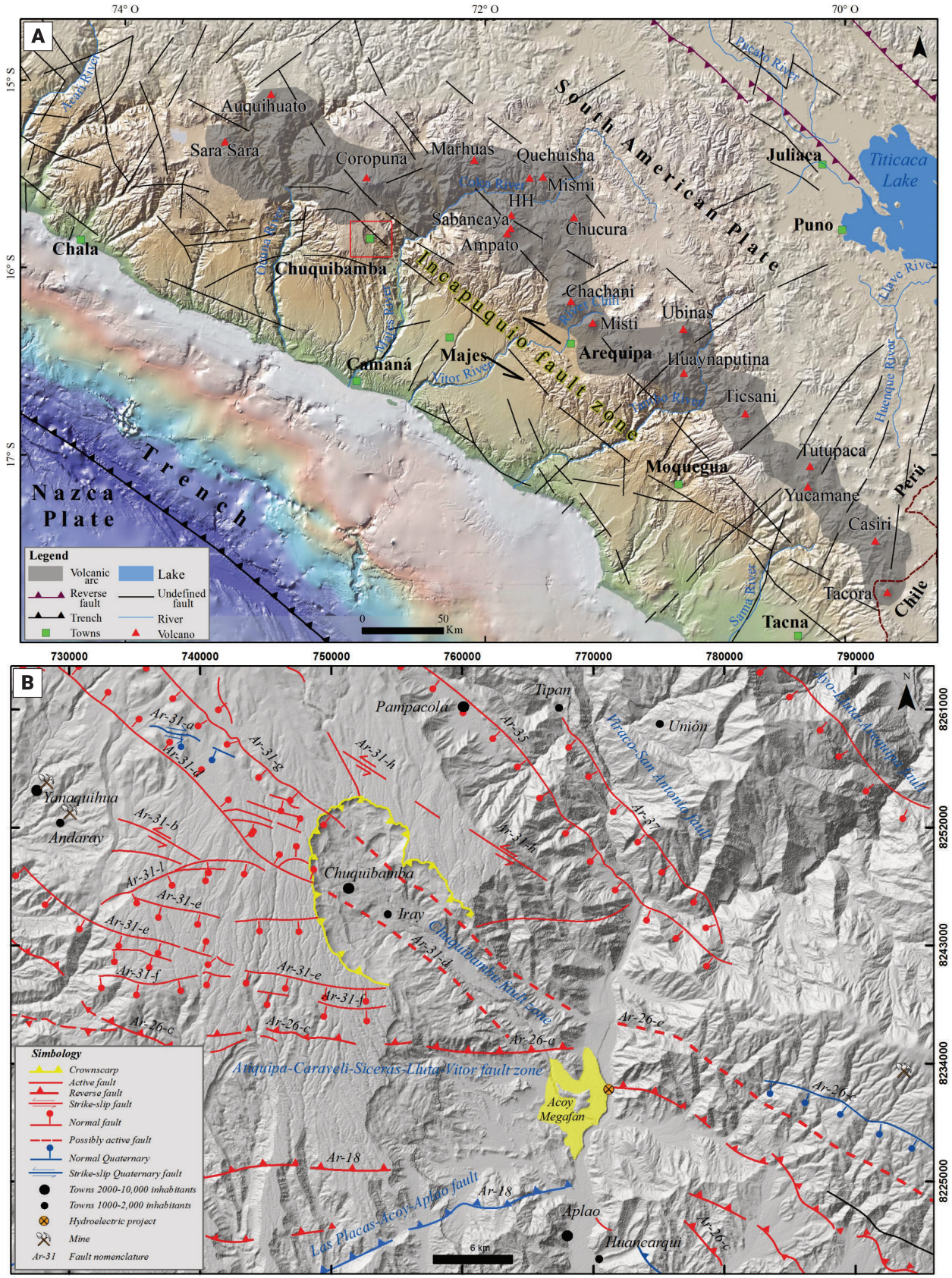

Figure 1. A) Regional map of the Andes Cordillera, the Western Cordillera, the location and extension of the Central Andes, and the study area (square). Red triangles represent volcanoes of the Volcanic Arc (gray area) (Benavente *et al.*, 2010). B) Map of the tectonic framework of the Central Andes of Peru and the location of the Western Cordillera Domain along the Camaná-Majes-Colca basin. The main faults were taken from INGEMMET (2020). Notice that Chuquibamba is affected by the Incapuquio Fault System.

have fluctuated between 6.2 and 8.6 in magnitude (IGP, 2006; Alayo, 2007). The main focal mechanisms of the Incapuquio Fault megastructure correspond to a transcurrent tectonic environment with a left lateral component and a preferential NW-SE direction, associated with subduction in southern Peru (Tavera *et al.*, 2000; Margirier *et al.*, 2015; Rodríguez and Becerra, 2018).

4. Geological setting

To describe the geological setting of the Chuquibamba region, we first refer to the large Camaná-Majes-Colca basin that covers 5,500 km^2 (Figure 1B). This basin extends to the northeast up to the Colca River valley, with a depth of 1.5 to 2.5 km. The river cuts Jurassic to Lower Cretaceous metamorphic rocks and diorite plutons and sedimentary rocks of Late Cretaceous to Early Paleogene age (Thouret *et al.*, 2007) (Figure 2). To the SE of Chuquibamba, the Colca River (herein named the Majes-Camaná river) cuts Mesozoic rocks covered by the Moquegua group conglomerates of Paleogene to Lower Miocene age (Thouret *et al.*, 2016). Near the Pacific Ocean, the Camaná River cuts Paleogene rocks and conglomerates of the Moquegua Group that overlie metasediments and gneisses of the Precambrian basement (PE-gn), the oldest rocks in the area (Olchauski and Dávila, 1994). This basement is represented by a greenish-gray gneiss with a banded structure observed at sections 1108 and 1109 (Figure 3).

North of the town of Pacaychacra at section 1225, there is a sequence of limestones, andesites, and slates of the Lower and Middle Jurassic Socosani Formation. At sections 1111, 1112, and 1113 (Figure 3), granodiorites/tonalites are exposed, which belong to the Tiabaya Unit, being Upper Cretaceous in age. Approximately 2 km SE of the town of Iray (section 1115; Figure 3), conglomerates, sandstones, and ignimbrites of the Oligocene Caravelí Formation crop out (Olchauski and Dávila, 1994; Kasaka *et al.*, 2001; Thouret *et al.*, 2007, 2016).

Stratigraphically upward, there is a series of sedimentary rocks at several locations as follows: At site 1228 (Figure 3), northwest of Chiringay a heterolithological conglomerate composed of ignimbrite, granodiorite, andesitic and dacitic lavas, and metamorphic clasts crops out. At site 1108 (Figure 3), a succession of siltstone and sandstone layers with gravels is observed. The most complete succession of sedimentary rocks that overlies the greenschist is exposed in a quarry where it outcrops to the northwest of the Chuquibamba village (site 1109, Figure 3). The succession is highly fractured and faulted and consists of sandstones, conglomerates, and claystone (beige to red layers). The conglomerate is made of sandstones, gneiss, and limestone gravel clasts. These sediments crop out in the cliff

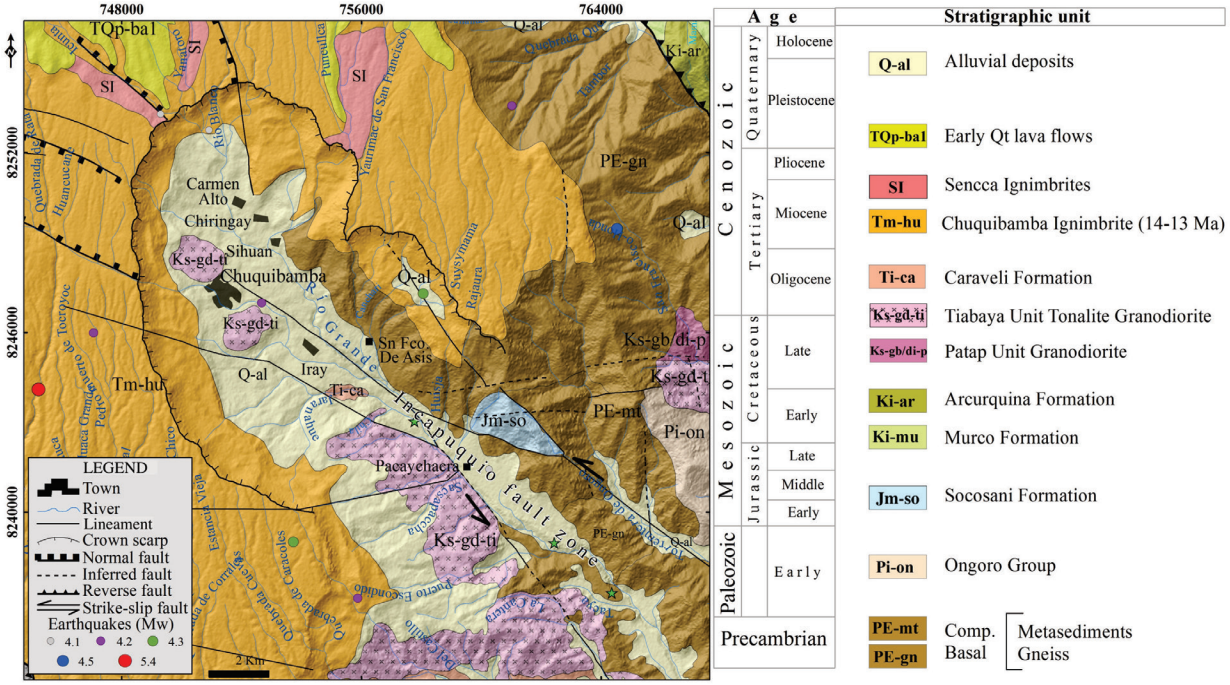

Figure 2. Geological setting of the Chuquibamba landslide, Western Cordillera, Peru. The map is from previous works (Olchauski and Dávila, 1994; Margirier *et al.*, 2015; INGEMMET, 2020). Notice that the Chuquibamba debris avalanche deposit is not mapped. The Incapuquio Fault System and minor faults were taken from Thouret *et al.* (2007, 2017), Margirier *et al.* (2015), and INGEMMET (2020). Colored dots in the map and legend represent earthquakes between 4 and 5.2 in magnitude that occurred in the area, according to the IGP (2006). **Appendix 1** lists earthquakes that have occurred in the region since 1960.

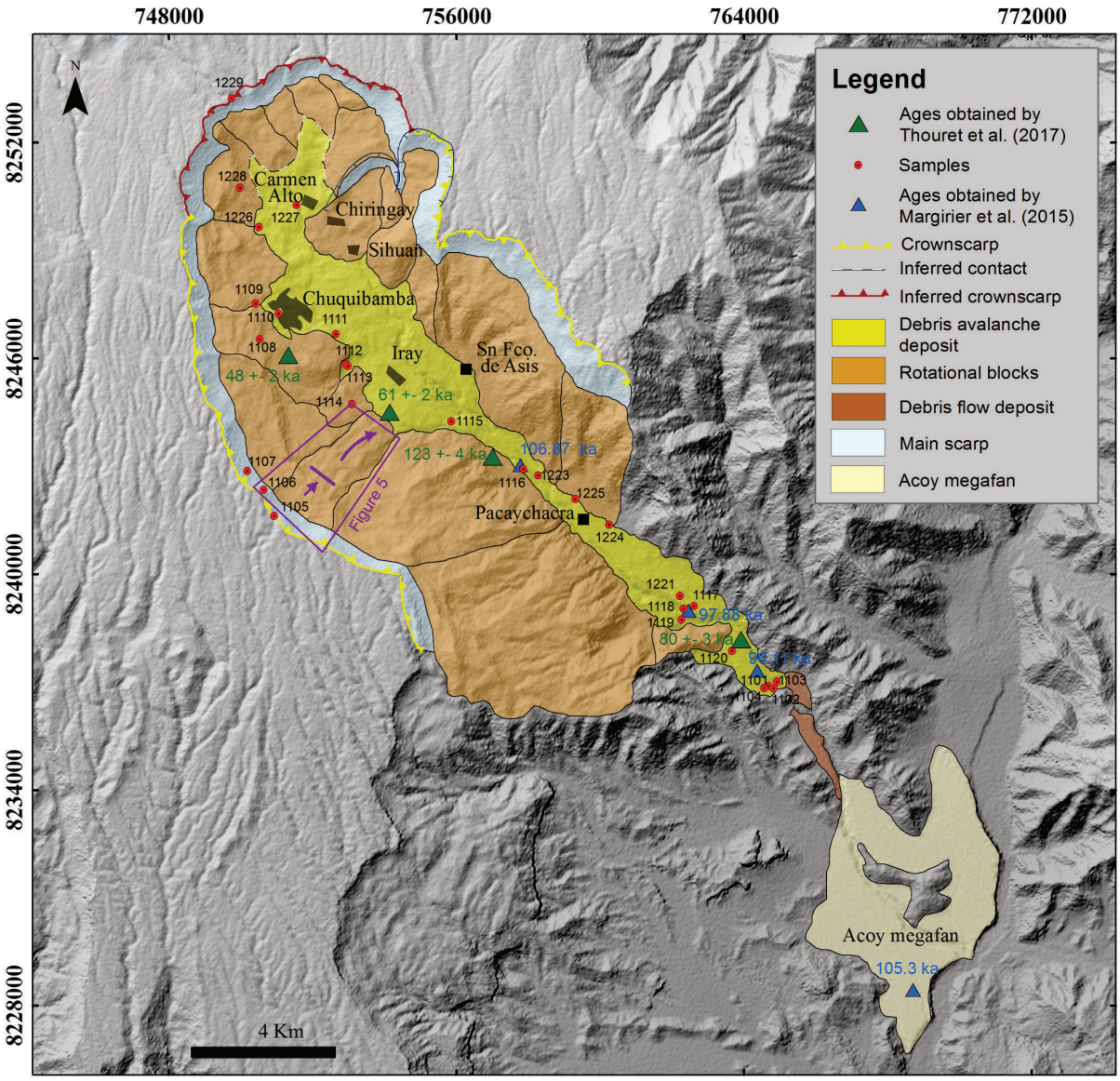

Figure 3. A) Digital Elevation Model (DEM) (gray pattern) scale 1:12,500 (with a 12.5 m horizontal resolution) of the Chuquibamba landslide and the debris avalanche deposit inside the Grande River valley. The map shows the elongated U-shaped and polylobate scar of the landslide, its distribution, and the shape of the rotated blocks (adapted from Margirier *et al.*, 2015), as well as the location of field descriptions (red dots). The purple contour line and arrows represent the rotated block diagram of Figure 5. Dates obtained using the ^{10}Be exposure measure are shown as blue triangles (Margirier *et al.*, 2015) and green triangles (Thouret *et al.*, 2017). The crown scarp associated to the debris avalanche deposit (inferred crownscarp) is shown as continuous red-color line, whereas the yellow crownscarp line is associated to the occurrence of rotated blocks sited at the base of the scarp and that were produced thousands of years after the main collapse presented in this study.

of the landslide along the road from Chuquibamba to Nevado Coropuna. A sedimentary formation of Tertiary (pre-Miocene) rocks has been reported between Chuquibamba, Ispacas, and Pampacolca (Alcalá-Reygosa *et al.*, 2015).

The most widespread rocks in the area comprise the Chuquibamba ignimbrite (14.3 – 12.7 Ma) (Olchauski and Dávila, 1994; Kasaka *et al.*, 2001; Thouret *et al.*, 2016), which consists of pinkish and grayish depositional units with abundant biotite that form a thick plateau (Wilson and García, 1962; Sánchez-Núñez *et al.*, 2020). On top of the Chuquibamba ignimbrite lies the Upper Sencca ignimbrite (1.8 - 2.2 Ma) and some of the Lower Sencca ignimbrite (2.82 - 5.13 Ma) (Thouret *et al.*, 2017)). These rocks are scattered and exposed on the "plateau" (high-land plain) to the NNW of the Chuquibamba landslide. On top of these ignimbrites, early Quaternary lavas (TQp-bal) of the Nevado de Coropuna volcanic complex (INGEMMET, 2020) crown the lithologic sequence (Figure 2).

Within the Chuquibamba depression at the bottom of the valley, a massive deposit is observed - described in this study as the Chuquibamba debris avalanche deposit (Figure 3). The

first description of the Chuquibamba landslide was reported by Olchausky and Dávila (1994). They classified this deposit as a landslide with gentle slopes, forming a valley carved out by the Grande River, a tributary of the Majes River, with an NW-SE orientation, which is consistent with the northwest orientation of the fault system. Kasaka *et al.* (2001) described the Chuquibamba landslide as a broad valley shaped by the different stages of erosion, presenting wide valleys with steep topography. On the geological map of INGEMMET (1998), it appears simply as alluvial deposits (Figure 2).

5. Landslide characteristics

5.1 Morphology

The Chuquibamba landslide (Figures 3 and 4A) is located within the Camaná-Majes-Colca River basin that is drained by the Camaná River, which empties into the Pacific Ocean. The most outstanding morphological feature of this basin is its wide and elongated U-shaped crown scarp of the Chuquibamba landslide (Figures 2, 3, and 4). It has a 37° NW-SE orientation parallel to the Incapuquio regional fault system. This system is a sinistral strike-slip fault with NW-SE oriented conjugated faults (Jacay *et al.*, 2002; Margirier *et al.*, 2015), which affect the landslide area, as seen in Figure 2. The upper part of the collapse area is affected by normal faults that are perpendicular to the slide direction (Jacay *et al.*, 2002). The lower part of the collapse area is dominated by strike-slip faults that limit tilted or rotated blocks oriented in various directions (Margirier *et al.*, 2015).

The head of the crown scarp has a maximum elevation of 3,900 m, exposing Miocene ignimbrites that form the pampa. The edges of the crown scarp extend downslope to elevations of ca. 2,900 m on both sides of the valley. The U-shaped (polylobate) crown scarp has a perimeter of ca. 40 km and has variable widths that range from 8.5 to 10.2 km (Figures 2 and 4A). The apex of the scarp has vertical cliffs to steep slopes (≥ 70°), then the slopes become smoother (~ 25°) (Figure 4A). The scarp depth varies from 300 to 1,000 m. The central part of the U-shaped scarp exposes the basal Precambrian gneiss and the Cretaceous granodiorites from the Tiabaya Unit (Figure 2).

The debris avalanche deposit is constituted by three facies, the most proximal is the block facies starting at an altitude of 3,270 masl and extends to an altitude of 2,537 masl; the mixed facies starts at 2,518 masl and continues until an altitude of 1,740 masl; whereas the matrix facies outcrops from altitudes of 1,720 and 1,167 masl (Figure 3). The front of the debris avalanche deposit is located at an altitude of 1,150 m, with 35 m-thick and has semi-vertical walls (Figure 4B-E). The toe has a lobular shape that is limited in its front by a talus deposit. The deposit has an H/L = 0.12, which is typical of dry debris avalanches elsewhere and consistent with non-volcanic debris avalanches described in the literature (Hayashi and Self, 1992; Legros, 2002). The DAD is incised by the main Grande River ravine that, in the deepest part, reaches ca. 25 m (section 1109; Figure 3). In this ravine, we found very well-exposed older rocks, the DAD, and reworked deposits on top (Figures 4B-E).

5.2. Extension and volume

The deposits associated with the Chuquibamba landslide are exposed along the Grande River (Río Grande) valley for about 22.5 km. The proximal outcrops occur at the base of the crown scarp, where the landslide is represented by rotated blocks (e.g., section 1228) (Figures 3 and 5), followed downflow by debris avalanche (Figures 4B-E; section 1101), debris flows, hyperconcentrated flows, fluviatile, and lacustrine deposits (Figs 6, 7, and 8). The widespread deposit is represented by the debris avalanche, discontinuously exposed along the Grande River throughout the villages of Chiringay, Chuquibamba, Iray, San Francisco de Asís, and Pacaychacra (Figures 3, 4B-C, and 9A-B). This deposit ends at ~10 km before the junction of the Grande and Majes rivers (Figure 7). The thickness of the deposit is quite variable, ranging from 130 m at section 1119 to 20 m at section 1226 (see Figure 3 for locations), averaging 70 m for the debris avalanche deposit. The whole Chuquibamba landslide (including the rotated blocks and distal deposits) covers an area of 192 km^2. We estimated a minimum volume of 39.74 km^3 (see Methods section for volume calculation details). This volume is comparable to that estimated by Margirier *et al.* (2015) and falls within the magnitude of large landslide deposits (Korup *et al.*, 2007; Paguican *et al.*, 2011; Dufresne *et al.*, 2016).

5.3 Type of movement and characteristic of rotated blocks

The landslide left an elongated U-shaped amphitheater that contrasts with the flat morphology of the extended pampa formed by ignimbrites of the Chuquibamba Formation. This tabular morphology causes the blocks to tilt in different directions and their origin is linked to rotational slides as proposed by Margirier *et al.* (2015). These authors concluded that the rotational slides obey extensional faults parallel to the crown scarp that reach several kilometers in length, and they occur as disaggregated blocks on their downhill sides, transitioning into smaller hummocks or even rock flows. Based on all these features Margirier *et al.* (2015) classified the landslide as rotational and dated the distal deposit at ~ 100 ka using the ^{10}Be exposure method (average of four samples).

Inside of the amphitheater and at the base of the cliff, we identified 17 coalescing rotated blocks with secondary scarps

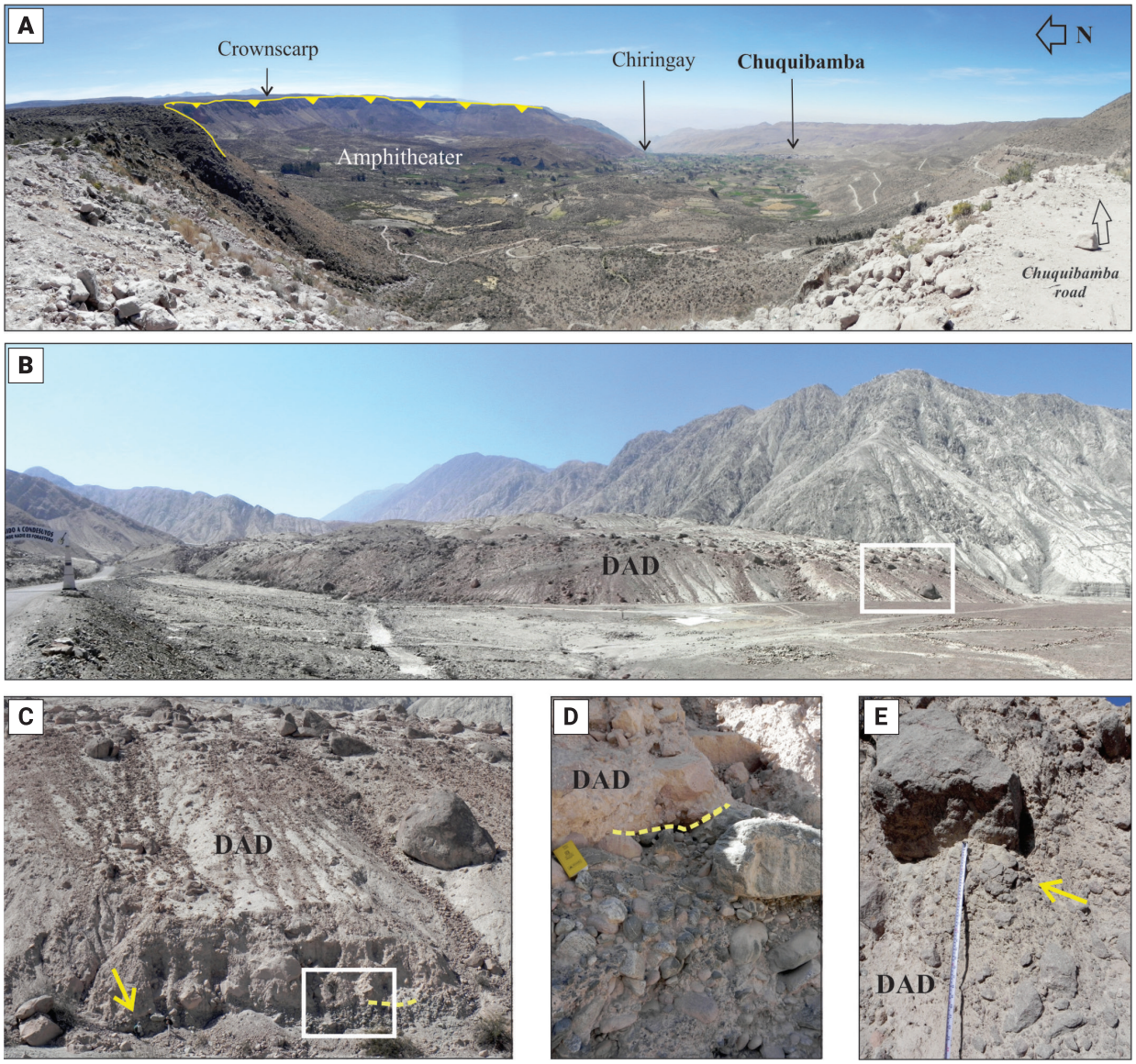

Figure 4. A) Panoramic view from the northwest of the Chuquibamba landslide that looks inside the Grande River valley. The picture was taken from site 1229 (3,690 m, see Figure 3) which exhibits the ignimbrites of the Chuquibamba Formation. The uppermost part of the scar is near vertical; B) General view from the southwest of the debris avalanche deposit (DAD) front at section 1101. The steep slope shows dispersed blocks and megablocks sustained by a finer-grained matrix—the white box shows area C; C) Blocks are angular to subangular in shape—the white box represents the limits of D (the yellow arrow points to the base of the deposit); D) The base of the DAD unconformably covers a gray conglomeratic bed; and E) Several blocks in the DAD display the typical jigsaw-fit structure of debris avalanche.

(Figure 3). These blocks have a recognizable shear surface, parallel to the axis of the crown scarp contour. They are rotated with respect to the edge of the cliff and display shear displacement (sliding) along the concave failure surface ("spoon shape") (Figure 5). Although the sliding surface is not perfectly circular, the incipient internal deformation of the displaced rocks suggests a rotational movement.

These slitted blocks are composed of Precambrian basal gneisses, late Cretaceous diorites, Caravelí granodiorites, and the Sencca and Chuquibamba ignimbrites (see Figure 2). Sections 1108, 1109, and 1228 show good exposures of metamorphic and faulted sedimentary rocks occurring at the base of the rotated blocks (Figure 10). For instance, at section 1228, there is a 20 m thick hummock (Figure 11) composed of sedimentary rocks (conglomerates) with primary stratification, covered by gray ignimbrites of the Chuquibamba ignimbrites. The best example of the Tertiary sedimentary succession occurs at section 1109, located 1.2 km to the northwest of the Chuquibamba village. At the base, this location exhibits a ≥ 1.5 m-thick green gneiss covered by a ~ 12-m thick sequence of alternated greenish beds of conglomerates, gray beds or lenses of coarse to fine-grained sandstones, and reddish claystones. A few meters to the right of

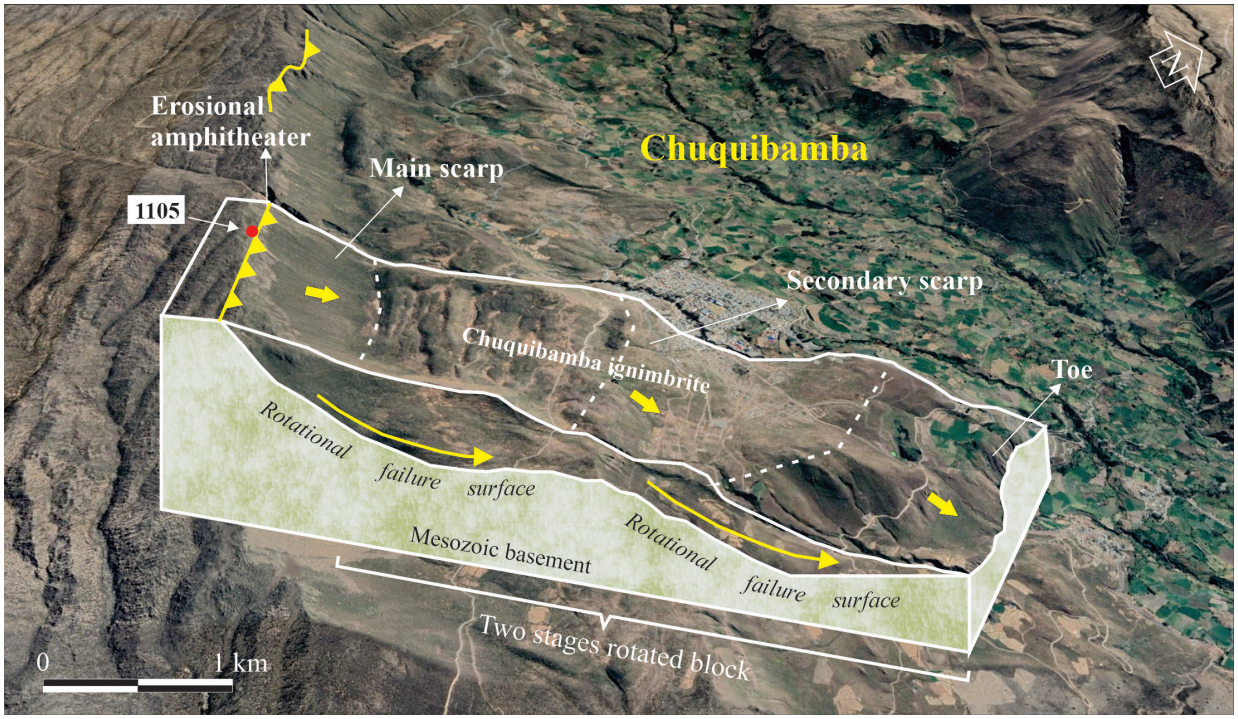

Figure 5. 3D-view Google Earth morphological block diagram of a rotational block with two stages of sliding on a retrogressive scarp. Interpretation was based on field descriptions. The diagram is a detailed view of a block showing the rotational fault surfaces on Mesozoic rocks, the sequence of movements, and the toe.

this exposure the uppermost green conglomerate (~ 10 m thick) shifts to a lithified heterolithological facies with sandstone, limestone, and gneiss fragments. Some rotational blocks show a retrogressive fault line, including the main scarp, and secondary scarps. At the end of the block, there is a toe-like morphology that comprises a lobe of accumulated material (Figure 5), attesting to a retrogressive movement (as previously reported by Thouret *et al.*, 2017).

In addition, based on the morphology of the huge landslide scar, the polylobate amphitheater of the slide mass, and its depositional features, we also classify the Chuquibamba landslide as a complex large-scale (3.9×10^{10} m^3) slope movement (Cruden, 1991; Dikau *et al.*, 1996a; Dade and Huppert, 1998; Paguican *et al.*, 2014; Margirier *et al.*, 2015; Thouret *et al.*, 2017 and Strom *et al.*, 2019).

6. Debris Avalanche Deposit (DAD)

At least 20 locations of the deposit can be seen in Figure 9A-B, which correlate to the units exposed along the Grande River valley. As described in previous studies of debris avalanches worldwide (e.g., Hewitt, 2009; Godoy *et al.*, 2012; Weidinger *et al.*, 2014; Dufresne and Dunning, 2017) we divided the deposits into different facies as a function of distance. The DAD is confined to the lower parts of the Grande River valley, and it is exposed for about 22.5 km from 3,900 to 1,167 masl with its main front located at ~ 10 km upstream of the Majes River. The DAD, as well as associated volcaniclastic deposits, have been described in 21 sections (Figure 9). Together, it covers an area of 33.64 km^2 with a minimum volume of 0.72 km^3 (see the Methods section for volume estimation details).

In this study, we recognize three facies of the deposit (blocks, mixed, and matrix) and we followed the terminology of Hungr *et al.* (2014), Weidinger *et al.* (2014), and Dufresne *et al.* (2016, 2017), as described next.

6.1. Block facies

This facies crops out from altitudes of 3,270 m (section 1227) to 2,537 m (section 1114) up to 5 km from the crown scarp (Figures 3 and 9). This facies exposes megablocks (hummocks ≥ 15 m) constituted by pink and gray ignimbrites and andesitic lavas (sections 1226 and 1227). Some megablocks remain intact with jigsaw-fit puzzle structures formed by angular blocks with scarce intra-clast matrix (Figure 12A). The deposit in the block facies discordantly covers gneisses and a sand-conglomerate-shale succession of the Precambrian basal complex (section 1110), as well as rocks of the Upper Cretaceous granodiorite of the Tiabaya Formation (sections 1111, 1112, and, 1113). One of these extremely elongated shattered blocks of the DAD occurs at section 1111, which is covered by hyperconcentrated and debris flow deposits (Figure 6).

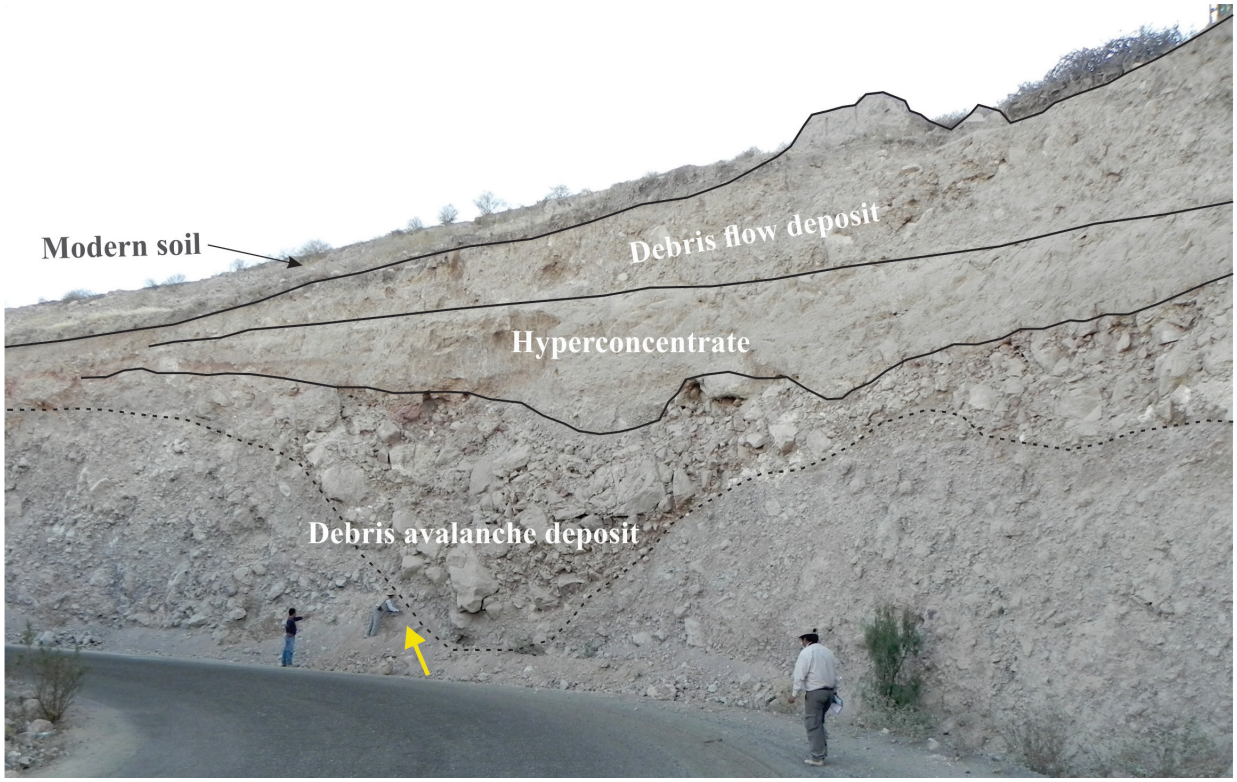

Figure 6. View to the northwest of the block facies showing a large jigsaw-fit megablock of the debris avalanche (DAD) exposed towards the upper part of the deposit. The DAD shows <1 m thick angular shattered blocks supported by a fine-grained coarse sandy matrix. The deposit is overlain by thick hyperconcentrated (HFD), and debris flow deposits (DFD).

The exposures located in the northwest part of the block facies have a large proportion of blocks (80 – 90%) in comparison with the intra-clast matrix. A typical exposure of the block facies (section 1226, in Figure 12A and D) shows angular to subangular shattered blocks representing ca. 90% of the outcrop. The granulometric distribution of the block facies is polymodal (modes at -11 to -7, -4, and 1) with a leptokurtic kurtosis (0.87) and a mixture of extremely poorly selected clasts ($\sigma i = 4.79$).

6.2. Mixed facies

The mixed facies extends between 5 to 15 km from the crown scarp between altitudes ranging from 2,518 m (section 1111) to 1,740 m (section 1224) (Figure 3 and 9). The deposit appears as elongated hills that are aligned in the direction of the flow (NW-SE). It has a variable thickness ranging from 20 to 60 m. This facies overlies the granodiorites-diorites of the Tiabaya Formation in addition to the Precambrian gneisses and metasediments (sections 1115 to 1123). To the northwest of Pacaychacra, the deposit also covers the Upper Cretaceous granodiorite of the Tiabaya Unit (sections 1114, 1115, 1116, and 1123). In these areas, the mixed facies extends laterally and longitudinally, showing scarce dispersed blocks that are set in a more abundant matrix (Figure 12B). The deposit is characterized by multicolored rock blocks (red, pink, green, and beige) consisting of ignimbrites (a pink biotite-bearing ignimbrite being the most common), but also andesitic lava blocks, and conglomerate blocks. The outcrops present megablocks (≥ 4 m) of pink ignimbrite, fine-grained breccia of ignimbrite, and red fragments of conglomerates. Some megablocks display jigsaw-fit puzzle structures with sub-angular forms within a scarce intra-clast matrix. We analyzed the structure of the mixed facies at seven locations with the best exposures. In general, the blocks represent between 40 and 60% of the deposit with respect to the matrix (Figure 12D). The granulometric distribution of the matrix is poorly sorted ($\sigma i = 4.0$) with a polymodal distribution (modes from -11, -8, -6, -5, -3, and 4), and with leptokurtic kurtosis (0.9).

6.3. Matrix facies

The transition between the mixed and the matrix facies is gradual, the proportion between blocks and matrix is variable,

as observed in other debris avalanche deposits (Reubi and Hernandez, 2000). For the DAD, we were able to establish that the matrix facies occur between 15 and 22.5 km at the frontal lobe (Figures 4C-D, 3 and 9). Therefore, it extends 7 km downstream to the southeast of the town of Pacaychacra. This facies occurs between altitudes of 1,720 and 1,167 m where it overlies the Precambrian gneisses and metasediments (sections 1101 to 1104) (Figure 9). The deposit consists of a mixture of smaller rock fragments derived from various parts of the source and the substrate (Figure 7A).

We analyze the structure and texture of eight selected outcrops of the matrix facies (Figure 12C). In these locations, the outcrops are composed of subrounded to rounded blocks that represent from 20 to 35 vol.% of the deposit. The deposits are massive, pink to beige in color, with clasts embedded in a medium to coarse sand matrix. The matrix represents ca. 80 vol.% of the deposit. Its granulometric distribution is poorly sorted ($\sigma i = 4.0$), polymodal (modes from -9, -7, -3, 2, 4), with platykurtic kurtosis (0.8) (Figure 12D).

7. Debris flow and hyperconcentrated flow deposits

A thick sequence of stacked debris flow deposits is exposed a few meters beyond the edge of the debris avalanche and all along the Grande River valley as a series of flat terraces (Figure 7B-D), stratigraphically above the DAD. Close to section 1101 (see Figure 3 for location), these deposits are observed to be separated by sharp, flat contacts, each unit being massive with metric-size boulders embedded in a coarse sandy matrix.

We identify eleven outcrops in which the debris avalanche is covered by heterolithologic debris flows or hyperconcentrated flows, fluvial and lacustrine deposits (e.g., sections 1104, 1225, 1227) (Figures 9 and 8), even in proximal areas of the deposit

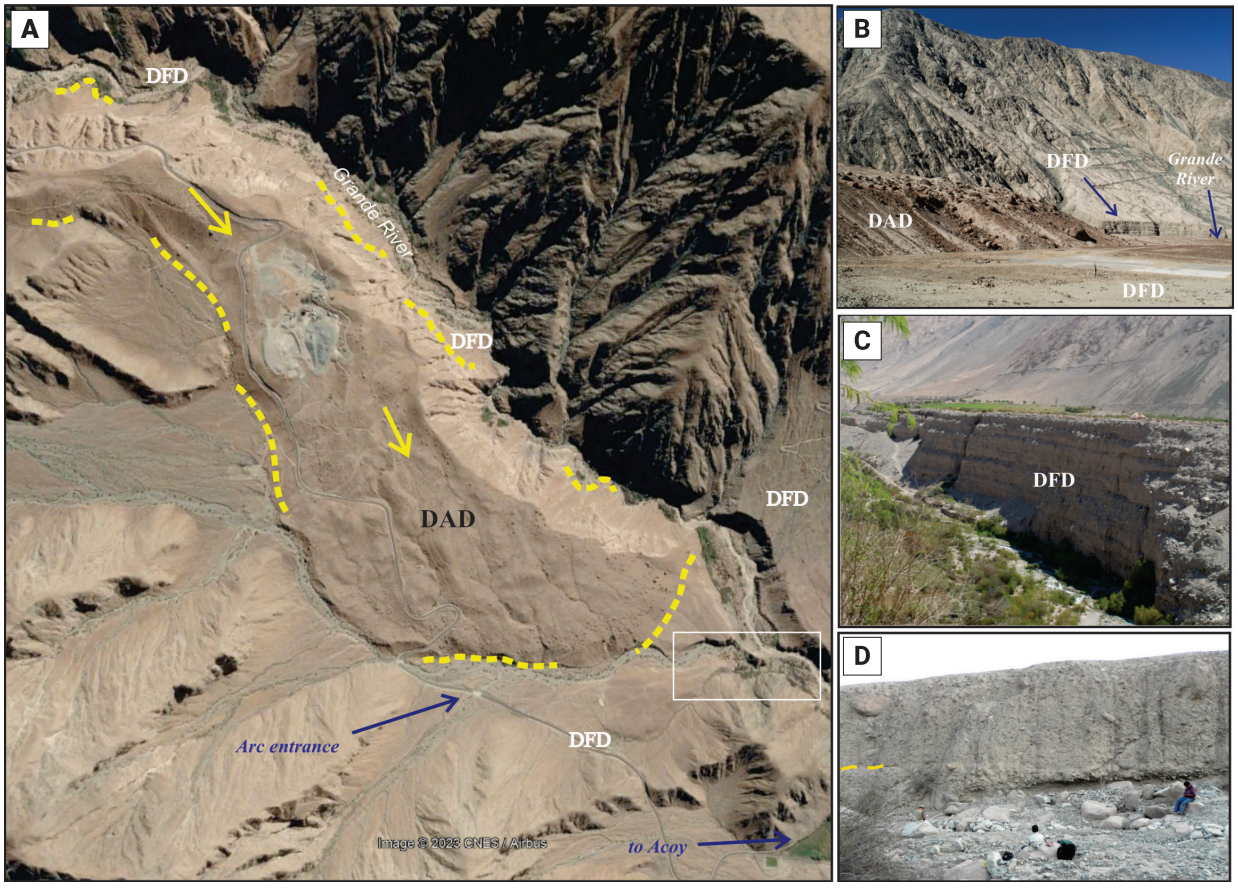

Figure 7. A) Aerial view of the distal tip of the debris avalanche deposit (DAD) showing its front and lateral parts (dashed yellow lines) and terraces with debris flows (DFD), and fluviatile deposits. Notice the dispersed boulders on top of the DAD. Solid rectangle shows the area where B - D photos were taken. B) Lateral view from the southwest of the Debris Avalanche Deposit (DAD) front bounded by Debris Flow Deposits (DFD) that occurred at a flat terrace in the background and on the foreground part of the picture; C and D) General view from the northwest of a stacked sequence of Debris Flow Deposits (DFD) composed of massive beds with boulders in a finer-grained matrix, each bed separated by nearly horizontal sharp boundaries.

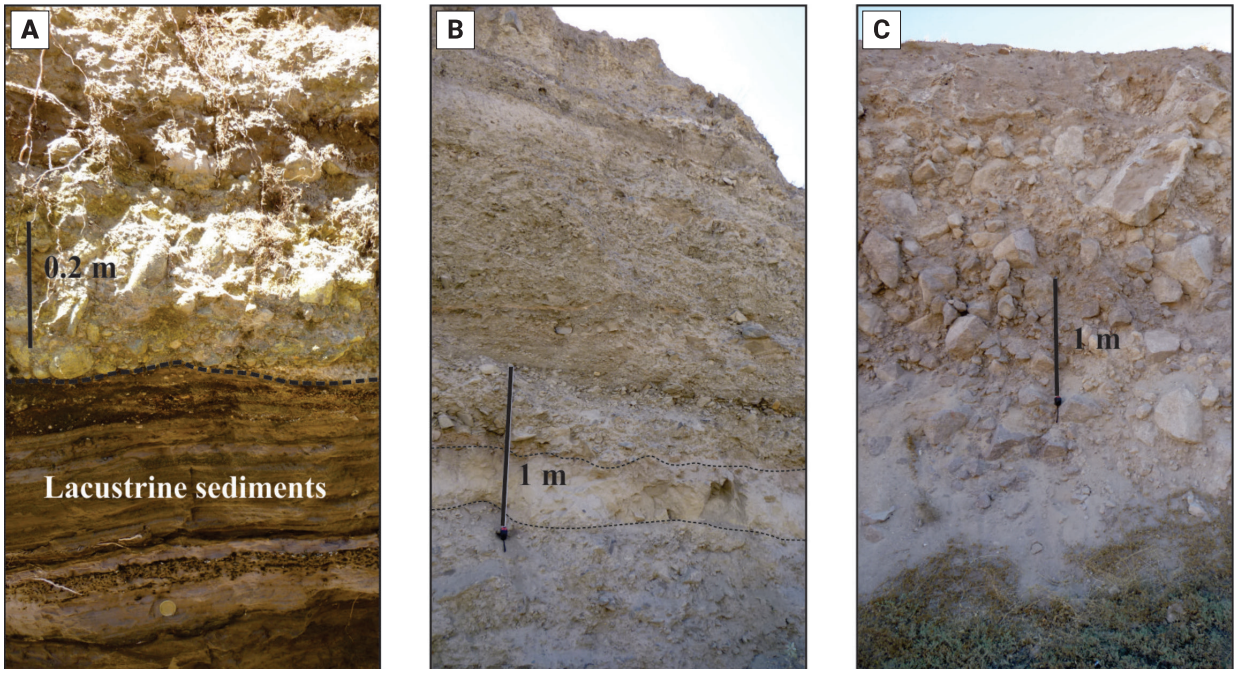

Figure 8. A) The contact between a sequence of lacustrine deposits (bottom) of ~ 0.80 m, overlain by a 1.20 m thick debris flow that represents the upper part of section 1227. B) Section 1124 showing a sequence from the base to the top of a light gray 2.10 m-thick debris flow, with subangular fragments of calcareous sandstone; it is overlain by a hyperconcentrated 0.55 m-thick deposit with a predominance of the matrix (silts); at the top, there is an ~ 4 m-thick debris flow deposit with imbricated clasts and sand lenses. C) Section 1221 shows an ~ 10 m-thick massive debris flow deposit, with metric, subangular, and poorly sorted fragments. It shows the correlation of eight stratigraphic columns in which debris flows, fluvial, and hyperconcentrated flow deposits cover the debris avalanche deposit.

(section 1227) (Figure 6). In section (1224), the outcrop exhibits (from its base) a 2.1 m-thick heterolithologic debris flow deposit, which is overlain by a 0.55-m-thick hyperconcentrated flow deposit (silt to clay particles), while being covered by a white ash likely associated with the 1600 CE Huaynaputina volcanic eruption (Witze, 2008; Fei *et al.*, 2016).

8. Discussion

8.1. Origin of the Chuquibamba Landslide

The Chuquibamba area is situated in the Plio-Quaternary Central Volcanic Zone (CVZ) of the Andes in southern Peru. The region has suffered numerous highly destructive landslides that have modified the terrain's morphology (Thouret *et al.*, 2017, Benavente *et al.*, 2022). Large earthquakes (M > 6; Tian *et al.*, 2019) associated with active tectonics, may induce landslides (Korup, 2004; Brideau *et al.*, 2009; Barth, 2013; Crosta *et al.*, 2015; Tapia-Baldis *et al.*, 2018). Between 1906 and 1972 there were thirteen earthquakes with magnitudes > 7 Mw in the Peruvian Andes (Dorbath *et al.*, 1990). Among these events, the 1970 earthquake (Mw ~ 7.9) triggered the collapse of the western face of the Nevado de Huascarán glacier in the Cordillera Blanca, killing ca. 6,000 people and burying the towns of Yungai and Ranrahirca (Evans *et al.*, 2009). Large earthquakes (magnitudes > 7) are associated with the subduction of the Cocos and South America plates, and they may combine with complex fault systems, such as in the case of the Chuquibamba area, to trigger landslides in southern Peru. The Chuquibamba landslide is aligned to the NW-SE-trending sinistral transcurrent Incapuquio-Challaviento fault system (Jacay *et al.*, 2002; Stern, 2004). It has a crown scarp with an elongated U-shaped (polylobate) typical of fault-related landslides, as described by Acocella (2021). By analyzing the modern seismicity in the region, some earthquakes have been reported to have epicenters along the trace of the Incapuquio-Challaviento fault system (Benavente *et al.*, 2017; IGP, 2006), which seems to be presently active. Thouret *et al.* (2017) concluded that the asymmetric topography of the Chuquibamba amphitheater, with its western flank twice as long as its eastern flank, may be the result of a half-graben along the strike-slip N130º E faults. They further mentioned that the polylobate form of the scar may be the result of the faults that strike N130º E and N160º E. These authors attributed the collapse to the tectonic setting aided by sapping at the base of the ignimbrites in contact with the sedimentary and metamorphic rocks. We agree with this latter conclusion because our field analyses corroborate that the Oligocene sedimentary rocks

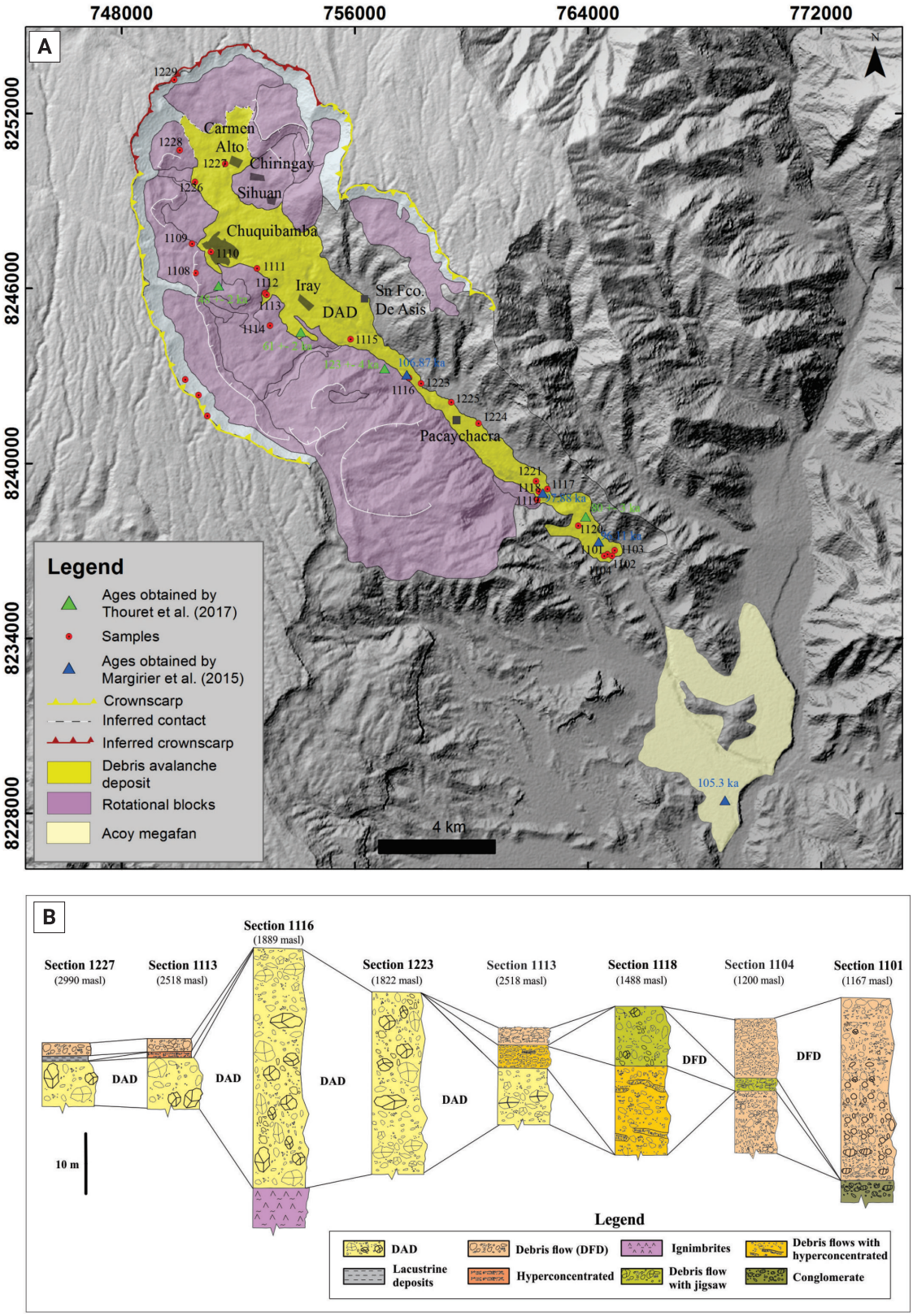

Figure 9. A) Digital Elevation Model (DEM) showing the rock avalanche extension, and the sample sites on the deposit with the main debris avalanche units of Thouret *et al.* (2017). (B) Stratigraphic correlation of lithologic columns along the Chuquibamba rock avalanche deposit. Throughout the deposit, the thickness varies from 7 to 40 m. The debris avalanche deposit is covered by debris flows, hyperconcentrated flows, lacustrine, and fluvial deposits.

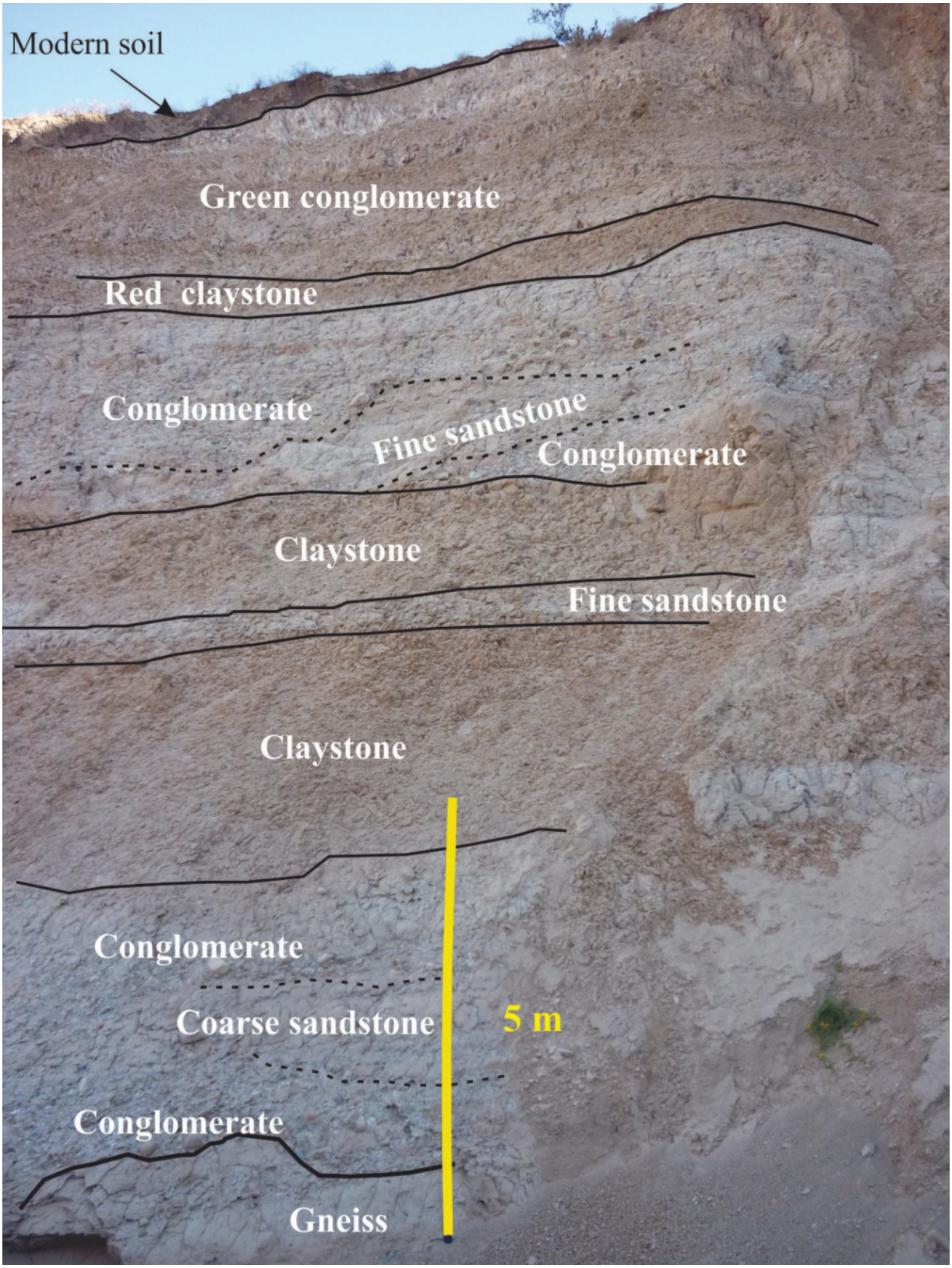

Figure 10. Closeup look of the stratigraphic section 1109 that exhibits a succession of stratified green conglomerates, gray sandstones, and reddish claystones covering the Paleozoic gneiss.

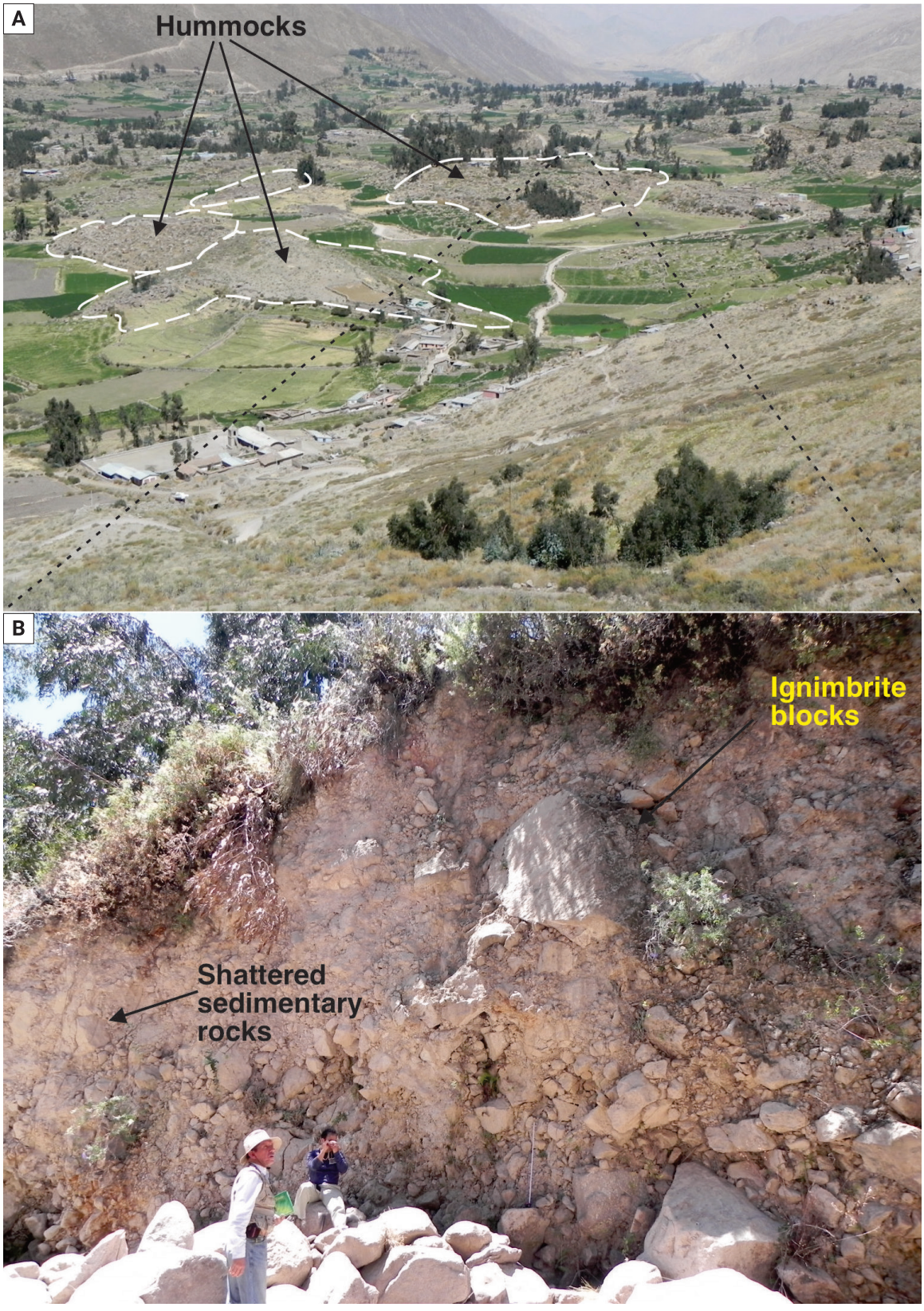

Figure 11. A) Panoramic view of proximal facies of the debris avalanche deposit showing the hummocky topography; B) Detail of the internal hummock structure showing some shattered blocks of sedimentary rocks and ignimbrites at site #1228 (see Figure 9 for location sites).

(conglomerates, sandstones, and claystones) are highly weathered and faulted, as observed near Chiringay village. Based on the elongated asymmetric morphology of the crown scarp, the trace of the Incapuquio-Challaviento fault system, and its intersection with the N160º E faults and the associated modern seismicity, we believe that the Chuquibamba landslide could have been initiated by tectonic activity in the region, as suggested by previous authors (e.g., Crosta *et al.*, 2015; Thouret *et al.*, 2017; Delgado *et al.*, 2022), leading to progressive uplift of the crust and thus, large magnitude earthquakes. Because of the dry nature of the debris avalanche deposit, we rule out other causes of the collapse such as extreme rainfall (Scott et al, 2005; Bromley *et al.*, 2009; Sepúlveda *et al.*, 2014), glacial debuttressing (Guardamino and Drenkhan, 2016), intense hydrothermal alteration associated with the deposit (Siebert, 2002), and active volcanism since no other deposits have been associated to the avalanche (Glicken, 1996).

We estimate that the landslide remobilized an estimated volume of 39.74 km^3. This volume corresponds well with the missing rock volume (33.1 km^3) inside the crown scarp (Figures 3 and 4), a value similar to the volume of ~ 40 km^3 previously estimated by Margirier *et al.*, (2015). Similar landslides have been triggered by tectonic activity, major faults, rock weathering, and possible large magnitude earthquakes described along the Colca, Cotahuasi, Majes, and Cabanillas rivers, suggesting intense seismic activity in the past, hence promoting the frequency of large landslides in the region (Ericksen *et al.*, 1970; Evans *et al.*, 2009; Lara *et al.*, 2017; Thouret *et al.*, 2017; Sánchez-Núñez *et al.*, 2020). The approximately 20% difference between the deposit and the missing volume inside the crown scarp may be explained by bulking along the path of the debris avalanche, or due to dilation of the material during transport as described in the 1980 rock-slide of the Mount Saint Helens (Glicken, 1996).

8.2 Landslide and debris avalanche behavior

The Chuquibamba landslide started with the rupture of the slope in the pampa (listric fault) through the Chuquibamba and the Lower Quaternary Sencca ignimbrites as described by Thouret *et al.* (2017). These ignimbrites rest over highly fractured and faulted water-saturated sedimentary rocks that act as a displacement or weakness surface for the landslide. The Chuquibamba collapse generated the DAD by the disintegration of the collapsed material along the main Grande River valley as a massive flow controlled by gravity.

The deposits originated from the Chuquibamba landslide consist of three main facies: i) multiple rotational megablocks, ii) mixed dispersed blocks in a matrix, and iii) a distal facies with a lower proportion of blocks in the matrix. They all occurred during the same event, at different times, according to their degree of fragmentation and travel distance. The landslide and its deposit were produced by overlapping factors like lithological characteristics, stratigraphic order, substrate and topographic features which contributed to its emplacement dynamics, as suggested in other works (Dufresne *et al.*, 2018; Lin *et al.*, 2022), who described how the fracturing and fragmentation of blocks in rock avalanches are critical phenomena that occurs ubiquitously.

According to our morphological analyses and previous studies, we believe that the landslide occurred as follows: 1) firstly, the previously faulted rocks of the Incapuquio-Challaviento fault system failed by a combined effect of tectonic activity and sapping of the ignimbrite cover at the contact with the sedimentary and metamorphic rocks. Tectonic activity constantly affects the region through uplift, faulting, and associated earthquakes. The failure occurred along the NW-SE Incapuquio-Challaviento fault system, while detaching the uppermost succession of rocks made by the Chuquibamba ignimbrite (13.9 - 14.25 Ma) and the 2 Ma Lower Sencca ignimbrite down to the Oligocene sedimentary faulted rocks. This failure formed blocks that moved perpendicular to the fault zone; 2) next, by a progressive disintegration, the sliding mass transformed to a debris avalanche with deposition of megablocks (hummocks) in the proximal and middle reaches and a matrix-rich facies in the distal area.

Based on field observations of the DAD morphology with its steep front and lateral levees, and considering the internal structure of the deposit, we assume that the landslide occurred during a period of dry conditions that were very similar to those present nowadays. Therefore, the mass moved as a dry-rock avalanche. This is confirmed by the shattered texture of the deposit and the absence of pores, as well as its final morphology with its abrupt lobate front. We also observe that preserved stratigraphy, jigsaw-fractured blocks, or even cataclastic blocks with preserved outlines, do not suggest a collisional regime. Since the deposit of materials does not show significant fragmentation or mixing during propagation (Manzella and Labiouse, 2013), we propose a frictional regime for the Chuquibamba slide.

The landslide mass originated at the scarp failure with zero speed and started accelerating down the slope, gaining momentum. Along its path, the dry avalanche surmounted different obstacles and infilled the valley, causing its partial avulsion. After moving 13 km from the source, the dry rock avalanche overpassed a 20 m high obstacle for which we estimate a minimum speed by assuming wholly kinetic energy and transformed into potential energy with no frictional loss ($v=\sqrt{2gh}$). We considered $h = 2$ m, $g = 9.8$ m/s^2, resulting in ca. 20 m/s for the avalanche velocity. Downslope at the 20 km point (near the village of Pacaychacra), the debris avalanche was still capable of surmounting a 12 m hill, for which we estimate a minimum speed of 15 m/s. Therefore, at this distance, the moving mass had a significant

speed reduction before stopping at the 22.5 km mark. These speeds are within the range of other debris avalanches, such as in the 2017 Piz Cengalo-Bondo, SE Switzerland (25 – 50 m/s), Nevado Huascaran, Peru (50 – 85 m/s), the 2002 Kolka glacier rock-ice avalanche, Peru (60 – 80 m/s), and the Six des Eaux Froides rock avalanche, Switzerland (5 – 50 m/s) (Manzella, 2008; Pudasaini and Krautblatter, 2022). These speeds may be influenced by the original volume of the rock mass, its degree of weathering, pre-existing topography, slope, the morphology of the valley, and water-ice interaction.

8.3. Age, extent, and type of deposit

The age of the debris avalanche deposit has been reported in two different papers with different numbers and different interpretations of the event. Margirier *et al.* (2015) dated six boulders exposed on the surface of the DAD (describing by them as a debris flow deposit) at different locations (see Figure 9) by the cosmogenic ^{10}Be method, obtaining a range from 108.46 ± 10.2 to 96.11 ± 8.9 ka, with a weighted average age of 101.9 ± 5.5 ka for the deposit (Figure 13). Additionally, these authors dated a boulder exposed at the confluence of the Grande and Majes rivers (on the Acoy megafan; Figure 3), obtaining a ^{10}Be age of 105.3 ± 10.2 ka. On other hand, Thouret *et al.* (2017) reported ages for different parts of the Chuquibamba landslide that were described as units I to IV. Their deposit subdivisions were based on four ^{10}Be exposure ages of the deposits (see Figure 13). These DADs are: Unit I (48 ± 2 ka), Unit II (undated), Unit III (61 ± 2 - 80 ± 3 ka) and Unit IV (123 ± 4 ka). Based on the distribution of these units they proposed that the Chuquibamba landslide occurred as four retrogressive landslides. Next, they correlated their Unit III (80 – 60 ka) with the 101.9 ± 5.5 ka debris flow deposit of Margirier *et al.* (2015). By looking at the location of all the exposure ages of Unit III from Thouret *et al.*

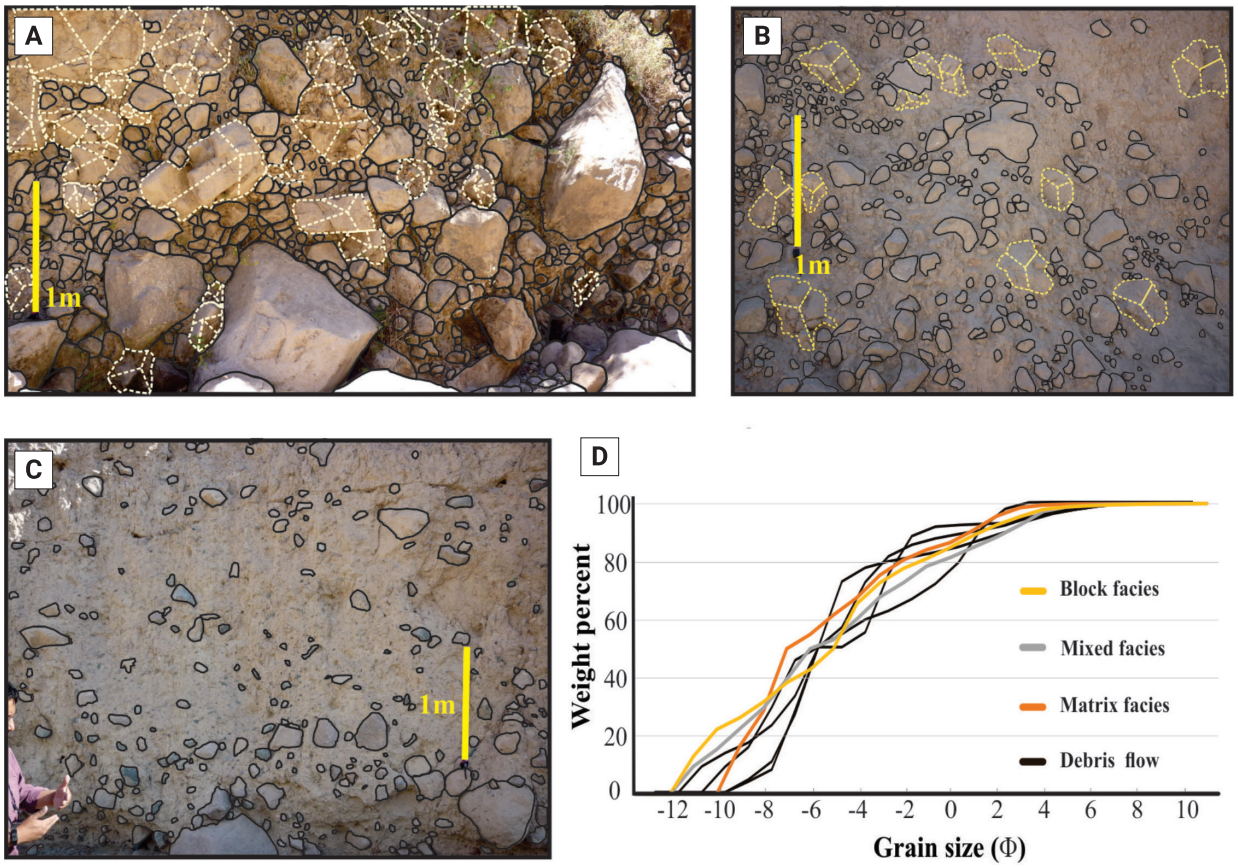

Figure 12. A) Aspects of the block facies of the Chuquibamba rock avalanche at section 1226. Notice the heterogeneity in the clast size of the deposit, the scarce fine-grained matrix, and the predominance of jigsaw-fit blocks. These blocks are shattered but still coherent with fragments that remain packed and closed together. B) The mixed facies at section 1113 contains circa 60% of subangular to subrounded blocks supported by a fine sandy matrix in both outcrops. Some jigsaw-fit clasts (dotted yellow lines) still occur but with smaller dimensions than in the block facies. C) The matrix facies in section 1101 has approximately 65 – 80 vol.% of fine particles. No jigsaw-fit clasts are preserved. D) Cumulative curves of selected samples, 1126 block facies, 1113 mixed facies, and 1101 matrix facies.

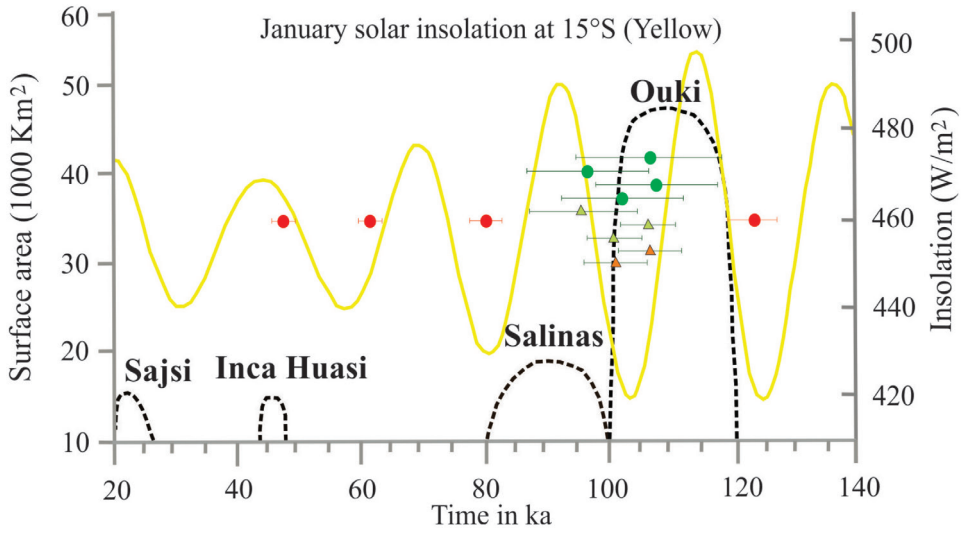

Figure 13. Reconstruction of some lake deposits (e.g. Ouki) in the central Andes and the January insolation yellow line (W/m² at 15° from Laskar, 1990) taken and modified from Placzek *et al.* (2009). The graph shows the ^{10}Be ages exposure ages of the Chuquibamba deposits of Margirier *et al.* (2015) (green circles) and Thouret *et al.* (2017) (red circles). Also shown are the ages of deposits dated in the Acoy megafan by Steffen *et al.* (2010) (green triangles), and Margirier *et al.* (2015) (orange triangles).

(2017) and Margirier *et al.* (2015), we have concluded that it is, in fact, the same deposit described in our study as a dry debris avalanche. However, we believe that the average age of 101.9 ± 5.5 ka of Margirier *et al.* (2015) better approximates the age of the DAD. The 101.9 ± 5.5 ka age is in good agreement with the OSL ages of Steffen *et al.* (2010) who dated sediments from the Acoy megafan between 107.0 ± 5.0 ka (at the base), and 101.6 ± 4.9 ka (near to the top) (Figures 3 and 7A). This period coincided with the Ouki wet climatic event that lasted between 120 and 98 ka in South America (Placzek *et al.*, 2006, 2009). Thus, we conclude that the giant landslide moved as a dry mass along the Grande River ravine for about 22.5 km and stopped ca. 10 km prior to the Acoy megafan, contrary to previous studies (Steffen *et al.*, 2010; Margirier *et al.* 2015) that associated the deposit to the Acoy megafan. We agree that Chuquibamba landslide occurred during the Ouki wet climatic event, as proposed by Margirier *et al.* (2015) but not necessarily during extreme rainfall or glacier outburst events. Based on the dry nature of the deposit we suspect that its collapse may have been triggered by an earthquake.

Sometime, after the emplacement of the dry avalanche, intense rains remobilized the DAD as debris flows along the Grande River ravine up to the Acoy megafan, debouching into the Majes river.

In the study of millennial and interannual timescales of the central Andes, Placzek *et al.* (2009) found that the arid environments of the western Andes are very sensitive to climate perturbations with significant changes in precipitation. This seems to be the case of the Chuquibamba failure that occurred during a dry period between precipitation events. Correlating the climate and the Chuquibamba landslide occurrence, it is evident that arid and semiarid environments existed in the region at the time of the collapse. There is strong evidence of exceptionally low precipitations on the western flank of the central Andes and the altiplano. By using the extremely high concentration of cosmogenic ^{10}Be, ^{21}Ne, ^{3}He, and ^{26}Al, Placzek *et al.* (2009), McPhillips *et al.* (2013, 2014) and Evenstar *et al.* (2017) claim that the landscape and climate have remained consistently arid climate over the entire Pliocene and Pleistocene.

We observed several flat terraces composed of a complex stack of debris flow deposits beyond the front of the DAD (Figure 7) and as patchy terraces exposed along the Grande River, which expose debris flows, hyperconcentrated flows, and fluvial deposits (Figures 7 and 8). Uplift rates in the Cotahuasi Valley (SE of Chuquibamba) have been estimated at 1.0 to 3.8 mm yr^{-1} (Thouret *et al.*, 2007, 2017), whereas subduction rates are on the order of 6 cm yr^{-1} having produced such exhumation and uplifting in this region (Hampel, 2002). The generation of these massive debris and hyperconcentrated flows by superficial water indicates that extraordinary rains occurred in the region, likely during the Ouki wet climatic event (120 ka – 98 ka) (Placzek *et al.*, 2006, 2009; Margirier *et al.*, 2015; Terrizzano *et al.*, 2017) aggrading the Acoy megafan at the confluence of the Grande and Majes rivers.

9. Conclusions

The field observations plus morphologic and granulometric analysis carried out in this study allow to reconstruct the sequence of events associated to the Chuquibamba *landslide* and deposits emplaced during the collapse (debris avalanche) and thereafter (debris flow, fluviatile and lacustrine deposit). We propose that Chuquibamba is a debris avalanche deposit, instead of a debris flow deposit as defined in previous works. We believe that the faulted and fractured rocks (due to the NW-SE strike-slip fault system) facilitated the collapse, which was triggered by earthquakes. The detachment surface followed the base of the Chuquibamba ignimbrite and fractured Tertiary rocks. This large landslide left a crown scarp with steep slopes and generated a debris avalanche deposit with three different facies: block facies (hummocky area), mixed facies, and matrix-dominated facies. Afterwards, temporal lakes formed in the hummocky area as recorded by lacustrine deposits. The debris avalanche deposit extends ~ 22.5 km from 3,900 to 1,167 masl. It covers an area of 33.64 km^2 with a minimum volume of 0.72 km^3. The resulting deposit has an H/L = 0.12, which is typical of dry debris avalanches elsewhere. The landslide occurred during dry conditions similar to the modern climate in the area and the deposit was confined to the Grande River ravine, yet never reaching the Acoy megafan. The avalanche occurred at about 102 ± 5 ka (Margirier *et al.*, 2015) and was followed by rainfall-generated debris and hyperconcentrated flows that traveled downstream, reaching the Acoy megafan as well as further downstream.

Some hundreds to thousands of years later, several collapses have occurred from the crownscarp (e.g. Unit I dated at 48 ± 2 ka by Thouret *et al.*, 2017). These collapses appear as rotated blocks at the base of the 40 km long scarp shaping the present morphology. The study of such large-magnitude landslides is of great importance because presently, in many regions of the Peruvian Andes, the conditions necessary to provoke a new collapse already exist, such as the observation of fractured rocks and the recent occurrences of large-magnitude earthquakes.

10. Acknowledgments

This work was partially supported by a 2011 grant to J.L. Macías from the Instituto Panamericano de Geografía e Historia (IPGH), the Instituto Geofísico del Perú, and the Instituto de Geofísica of the Universidad Nacional Autónoma de México. We appreciate the technical support of Guillermo Cisneros (image processing), Fabiola Mendiola (granulometric analyses), Felipe García (thin sections of rocks), and Gabriela Reyes (petrography and redaction of the manuscript). We appreciate the peer-review by two anonymous reviewers to improve and clarify the content of our contribution. Thanks to G.G. Buffett for the grammar review.

11. References

Acocella, V. (2021). Volcano flank instability and collapse. En A. Valerio Acocella (Ed.), *Volcano-Tectonic Processes* (pp. 205-244). Springer. doi: **https://doi.org/10.1007/978-3-030-65968-4**

Alayo, B.L. (2007). *Cronología histórica de los terremotos más destructivos en el Perú*. Centro de capacitación y prevención para el manejo de emergencias y medio ambiente, S.O.S Vidas Perú.

Alcalá-Reygosa, J., Palacios, D., Vázquez, L., & Zamorano, J. (2015). *Timing of maximum glacial extent and deglaciation from Hualca Hualca volcano (southern Peru) obtained with cosmogenic 36Cl.* [Presentación de paper]. European Geoscience Union, Vienna Austria.

Armijo, R., Lacassin, R., Coudurier-Cuveur, A., & Carrizo, D. (2015). Coupled tectonic evolution of Andean orogeny and global climate. *Earth Science Reviews*, 143, 1-35. doi: **https://doi.org/10.1016/j.earscirev.2015.01.005**

Barth, N.C. (2013). The Cascade rock avalanche: implications of a very large Alpine Fault-triggered failure, New Zealand. *Landslides*, 11 (3), 327-341. doi: **https://doi.org/10.1007/s10346-013-0389-1**

Benavente, C., Carlotto, V., & Castillo, B. (2010*). Extensión en el arco volcánico actual del sur del Perú. XV Congreso Peruano de Geología*. [Sesión de conferencia]. 2010 XV Congreso Peruano de Geología, Sociedad Geológica del Perú.

Benavente, C., Palomino, A., Wimpenny, S., García, B., Rosell, L., Aguirre, E., Macharé, J., Rodríguez Padilla, A., & Hall, S. (2022). Paleoseismic evidence of the 1715 C.E earthquake on the Purgatorio Fault in southern Peru: Implications for seismic Hazard in subduction zones. *Tectonophysics*, 834, 229355. doi: **https://doi.org/10.1016/j.tecto.2022.229355**

Benavente, C., Zerathe, S., Audin, L., Hall, S., Robert, X., Delgado, F., Carcaillet, J., & Team ASTER, (2017). Active transpressional tectonics in the Andean forearc of southern Peru quantified by ^{10}Be Surface exposure dating of an active fault scarp. *Tectonics*, 36(9), 1662-1678. doi: **https://doi.org/10.1002/2017TC004523**

Bowman, E.T., Take, W.A., Rait, K.L. & Hann, C. (2012). Physical models of rock avalanche spreading behavior with Dynamic fragmentation. Canadian Geotechnical Journal, 49(4), 460-476 doi: **https://doi.org/10.1139/T2012-007**

Brideau, M.A, Yan, M., & Stead, D. (2009). The role of tectonic damage and brittle rock fracture in the development of large rock slope failure. *Geomorphology*, 103(1), 30–49. doi: **https://doi.org/10.1016/j.geomorph.2008.04.010**

Bromley, G.R.M., Schaefer, J.M., Winckler, G., Hall, B.L., Todd, C.E., & Rademaker, K.M. (2009). Relative timing of last glacial maximum and late-glacial events in the central tropical Andes. Quaternary Science Reviews, 28(23-24), 2514-2526. doi: **https://doi.org/10.1016/j.**

quascirev.2009.05.012

Brügger, A., Tobias, R., & Monge-Rodríguez, F.S. (2021). Public perceptions of climate change in the Peruvian Andes. *Sustainability*, 13(5), 2677. doi: **https://doi.org/10.3390/su13052677**

Chayes, F.A. (1956). *Petrographic Modal Analysis: An Elementary Statistical Appraisal*. Wiley.

Crosta, G.B., Frattini, P., & Fusi, N. (2007). Fragmentation in the Val Pola rock avalanche, Italian Alps. *Journal Geophysical Research*, 112(F1), F01006. doi: **http://doi:10.1029/2005JF000455**

Crosta, G.B., Paolo, F., Elena, V., & Hermanns, R.L. (2015). The Cerro Caquilluco–Cerrillos Negros Giant Rock Avalanches (Tacna, Peru). En A. Lollino, G., *et al.* (Eds), Engineering Geology for Society and Territory-Volume 2. (pp. 921-924) Springer. doi: **https://doi.org/10.1007/978-3-319-09057-3_159**

Cruden, D.M. (1991). A simple definition of landslide. Bulletin of the International Association of Engineering Geology, 43, 27–29. doi: **https://doi.org/10.1007/BF02590167**

Cruden, D.M., Varnes, D.J. (1996). Landslide types and processes. Transportation Research, U.S. National Academy of Sciences, Spec. Rep. 247, 36-75

Cui, J., Gao, Ch., Zhang, Z., & Xiang, G. (2022). Description and dynamic analyses of the 1935 Luchedu Rock Avalanche in Sichuan, China. Hinddawi Geofluids, 2022, 5178989, doi: **http://doi.org/10.1155/2022/5178989**

Dade, W.B., & Huppert, H.E. (1998). Long-runout rockfalls. Geology, 26(9), 803-806. doi: **https://doi.org/10.1130/0091-7613(1998)026<0803:LRR>2.3.CO;2**

Delgado, F., Zerathe, S., Audin, L., Schwartz, S., Benavente, C., Carcaillet, J., Boulès, D., & Aster Team (2020). Giant landslide triggerings and paleoprecipitations in the Central Western Andes: The Aricota rockslide dam (South Peru). Geomorphology, 350; 106932, doi: **https://doi.org/10.1016/j.geomorph.2019.106932**

Delgado, F., Zerathe, S., Schwartz, S., Mathieux, B., & Benavente, C. (2022). Inventory of large landslides along the Central Western Andes (ca. 15°–20° S): Landslide distribution patterns and insights on controlling factors. J. South Am. Earth Sc. 116, 103824, doi: **https://doi.org/10.1016/j.jsames.2022.103824**

Dikau, R., Brunsden, D., Schrott, L., & Ibsen, M.L. (1996b). Landslide recognition, identification, movement and courses. Report no. 1 of the European Commission Environment Programme, Contract no. EV5V-CT-0454, John Wiley & Son.

Dikau, R., Cavallin, A., & Jäger, S. (1996a). Databases and GIS for landslide research in Europe. Geomorphology, 15 (3-4), 227-239. doi: **https://doi.org/10.1016/0169-555x(95)00072-d**

Dorbath, L., Cisternas, A., & Dorbath, C. (1990). Assessment of the size of large and great historical earthquakes in Peru. Bulletin of the Seismological Society of America. 80(3), 551-576. doi: **https://doi.org/10.1785/BSSA0800030551**

Dufresne, A., & Dunning, S. (2017). Process dependence of grain size distributions in rock avalanche deposits. Newcastle University ePrints. Landslides, 14, 1555-1563

Dufresne, A., Bösmeier, A., & Prager, C. (2016). Sedimentology of rock avalanche deposits Case study and review. Earth Sc. Rev. 163, 234-259, doi: **https://doi.org/10.1016/j.earscirev.2016.10.002**

Dufresne, A., Davies, T.R., & McSaveney, M.J. (2010). Influence of runout-path material on emplacement of the Round Top rock avalanche, New Zealand. Earth Surf. Process. Landf. 35, 190-201. doi: **https://doi.org/10.1002/esp.1900**

Dufresne, A., Dunning, S., & Becker, A. (2018). Evidence of rock avalanche emplacement dynamics recorded in grain size distributions and grain shape descriptors. Geophys. Res. Abstracts,20, EGU2018-1704

Ericksen G., Plafker, G., & Concha, J. (1970). Preliminary report on the geologic events associated with the May 31, 1970 Peru earthquake. Geol. Surv. Circular 639, Washington, D.C. 25p.

Evans, S.G., Bishop, N.F., Smoll, L.F., Murillo, P., Delaney, K.B., Oliver-Smith, A. (2009). A re-examination of the mechanism and human impact of catastrophic mass flows originating on the Nevado Huascaran, Cordillera Blanca, Peru in 1962 and 1970. Engineering Geology, 108: 96-118, doi: **https://doi.org/10.1016/j.enggeo.2009.06.020.**

Evenstar, L.A., Mather, A.E., Hartley, A.J., Stuart, F.M., Sparks, R.S.J., Cooper, F.J. (2017). Geomorphology on geologic timescales: Evolution of the late Cenozoic Pacific paleosurface in Northern Chile and Southern Peru. Earth-Science Reviews 171, 1-27. doi: **http://dx.doi.org/10.1016/j.earscirev.2017.04.004**

Fei, J., Zhang, D., & Lee, H. (2016). 1600 AD Huaynaputina eruption (Peru), Abrupt cooling, and epidemics in China and Korea. Adv. Meteor. 2016, 3217038, doi: **http://dx.doi.org/10.1155/2016/3217038**

Folk, R.L. (1974). Petrology of Sedimentary Rocks. Hemphill Publishing Co., Austin, Texas.

Freymuth, H., Brandmeier, M., & Wörner, G. (2015). The origin and crust/mantle mass balance of Central Andean ignimbrite magmatism constrained by oxygen and strontium isotopes and erupted volumes. Cont. Min. Pet. 169, 58. doi: **https://doi.org/10.1007/s00410-015-1152-5**

Glicken, H. (1996). Rockslide-debris avalanche of May 18, 1980, Mount St. Helens Volcano, Washington. US Geol. Surv. Open-File Rep. 96–0677, 1–90.

Godoy, B., Clavero, J., Rojas, C., & Godoy, E. (2012). Facies volcánicas de avalanchas de detritos del volcán Tata Sabaya, Andes Centrales. An. Geol. 39 (3), 394-406. doi: **http://doi:10.5027/andgeoV39n3-a03**

Guardamino, L., & Drenkhan, F. (2016). Evolución y potencial amenaza de lagunas glaciares en la Cordillera de Vilcabamba (Cusco y Apurímac, Perú) entre 1991 y 2014. Rev. Glaciares y Ecosistemas de Montaña, Instituto Nacional de Investigación en Glaciares y Ecosistemas de Montaña (INAIGEM) (1), 21-36.

Gunnell, Y., Thouret, J.C., Brichau, S., Carter, A. & Gallagher, K. (2010). Low temperature thermochronology in the Peruvian Central Andes: implications for long-term continental denudation, timing of plateau uplift, canyon incision and lithosphere dynamics. J. Geol. Soc. London,

167 (4), 803-815. doi: **https://doi.org/10.1144/0016-76492009-166**

Hampel, A. (2002) The migration history of the Nazca Ridge along the Peruvian active margin: a re-evaluation. Earth and Plan Sci. Lett., 203, 665-679. doi: **https://doi.org/10.1016/S0012-821X(02)00859-2**

Hayashi, J.N., & Self, S. (1992). A comparison of pyroclastic flow and debris avalanche mobility. J. Geophys. Res. 97, 9063-9071. doi: **https://doi.org/10.1029/92JB00173**

Hewitt, K. (2009). Catastrophic rock slope failures and late Quaternary developments in the Nanga Parbat-Haramosh Massif, Upper Indus basin, northern Pakistan. Quat. Sc. Rev. 28, 1055-1069, doi: **https://doi.org/10.1016/j.quascirev.2008.12.019**

Huggett, R.J. (2017). Fundamentals of Geomorphology. Routledge, Taylor and Francis Group.

Hungr, O., Leroueil, S., & Picarelli, L. (2014). The Varnes classification of landslide types, an update. Landslide, 11, 167-194. doi: **http://doi:10.1007/s10346-013-0436-y**

IGP (2006). Instituto Geofísico del Perú, Compendio estadístico de Prevención y Atención de Desastres. Sismos ocurridos en el Perú. Instituto Nacional de Defensa Civil, 7.

INGEMMET (1998). Instituto Geológico Minero y Metalúrgico, Mapa geológico escala 1:100 000 digital versión. Ministerio de Energía y Minas.

INGEMMET (2020). Instituto Geológico Minero y Metalúrgico, Mapa Tectónico Generalizado escala 1:4 000 000 digital versión. Ministerio de Energía y Minas. **https://es.calameo.com/read/0044619141ef68ef33ba9**

Inman, D.L. (1952). Measures for describing the size distribution of sediments. J. Sed. Res. 22, 125-145.

Iverson, R., & Denlinger, R. (2001). Flow of variably fluidized granular masses across three-dimensional terrain 1. Coulomb mixture theory. J. Geophys. Res. 106(B1), 537-552. doi: **https://doi.org/10.1029/2000JB900329o**

Jacay, J., Sempere, T., Husson, L., & Pino, A. (2002). Structural Characteristics of the Incapuquio fault system, southern Peru. Andean Geodynamics, 5th International Symposium Toulouse, France. Extended abstracts 319-321

Kasaka, R., Arias, H., Farfán, E., González, E., Minaya, A., & Campano, J. (2001). Evaluación de peligros de la ciudad de Chuquibamba. Universidad Nacional de San Agustín de Arequipa, Proyecto PER 98/018 PNUD-INDECI 89 p.

Korup, O. (2004). Geomorphic implications of fault zone weakening: Slope instability along the Alpine Fault, South Westland to Fiordland. NZ J. Geol. Geophys. 47, 257–267. doi: **http://doi:10.1080/00288306.2004.9515052**

Korup, O., Clague, J., Hermans, R., Hewitt, K., Strom, A., Weidinger, J. (2007). Giant landslides, topography and erosion. Earth Planet Sci. Lett. 261, 578–589. doi: **https://doi:10.1016/j.epsl.2007.07.025**

Lara, J., Gómez, J., Sánchez-Núñez, J., & Saucedo, R. (2017). Avalanchas de escombros en el complejo volcánico Sillapaca: Una herramienta para la gestión sostenible del territorio. Espacio y Desarrollo, 30, 193-208. doi: **https://doi.org/10.18800/espacioydesarrollo.201702.008**

Laskar, J. (1990). The chaotic motion of the solar system: A numerical estimate of the chaotic zones. Icarus, 88, 266–291.

Legros, F. (2002). The mobility of long-runout landslides. Engin. Geol. 63, 301-331. doi: **https://doi.org/10.1016/S0013-7952(01)00090-4**

Lin, Q., Wang, Y., Xie, Y., & Deng, K. (2022). Multiscale effects caused by the fracturing and fragmentation of rock blocks during rock mass movement: implications for rock avalanche propagation. Nat. Haz. Earth Syst. Sc. 22, 639-657, doi: **https://doi.org/10.5194/nhess-22-639-2022**

Manzella, I. (2008). Dry rock avalanche propagation: Unconstrained flow experiments with granular materials and blocks at small scale. [Tesis de doctorado]. École Polytechnique Fédérale de Lausanne, Suisse.

Manzella, I., & Labiouse, V. (2013). Empirical and analytical analysis of laboratory granular flows to investigate rock avalanche propagation. Landslide, 10, 23-36, doi : **http://10.1007/s10346-011-0313-5**

Margirier, A., Audin, L., Carcaillet, J., Schwartz, S., & Benavente, C. (2015). Tectonic and climatic controls on the Chuquibamba landslide (western Andes, southern Peru). Earth Surf. Dynam., 3, 281-289, doi: **https://doi.org/10.5194/esurf-3-281-2015**

McPhillips, D., Bierman, P., & Rood, D. (2014). Millennial-scale record of landslides in the Andes consistent with earthquake trigger, Nat. Geosc. 7, 925-930, doi: 10.1038/NGEO2278

McPhillips, D., Bierman, P., Crocker, T., & Rood, D. (2013). Landscape response to Pleistocene-Holocene precipitation change in the Western Cordillera, Peru: ^{10}Be concentrations in modern sediments and terrace fills. J. Geophys. Res.: Earth Surface, 118, 2488-2499, doi: **http://doi:10.1002/2013JF002837,2013**

Mehl, K.W., & Schmincke, H.U. (1999). Structure and emplacement of the Pliocene Roque Nublo debris avalanche deposit, Gran Canaria, Spain. J. Volcanol. Geoth. Res. 94, 105-134 doi: **https://doi.org/10.1016/S0377-0273(99)00100-6**

Mergili, M., Santiago, C.I., & Moreiras, S. (2014). Causas, características e impacto de los procesos de remoción en masa, en áreas contrastantes de la región Andina. Cuadernos de Geografía, Rev. Colomb.Geog. 24 (2), 113–131.

Nadim, F., Kjekstad, O., Peduzzi, P., Herold, Ch., & Jaedicke, Ch. (2006). Global landslide and avalanche hotspots. Landslide, 3 (2), 159-173.

Olchauski, E., & Dávila, D. (1994). Geología de los cuadrángulos de Chuquibamba y Cotahuasi. Instituto Geológico, Minero y Metalúrgico del Perú (INGEMMET), Lima (Perú).

Paguican E.M.R., van Wyk de Vries, B., & Lagmay A.M.F. (2014). Hummocks: how they form and how they evolve in rockslide-debris avalanches. Landslides, 11, 67-80, doi: **http://doi:10.1007/s10346-012-0368-y**

Paguican, E.M.R., van Wyk de Vries, B., & Lagmay, A.M.F. (2011). Hummocks in large avalanches: how they form and what they mean. Geophys. Res. Abstract. 13, EGU2011-3437, EGU General Assembly.

Pfiffner, O., & Gonzalez, L. (2013). Mesozoic-Cenozoic Evolution of

the Western Margin of South America: Case of the Peruvian Andes. Geosc. 3, 262-310, doi: doi:10.3390/geosciences3020262

Placzek, C., Quade, J., & Patchett, P.J. (2006). Geochronology and stratigraphy of late Pleistocene lake cycles on the southern Bolivian Altiplano: Implications for causes of tropical climate change. Geol. Soc. Am. Bull. 118(5-6), 515–532, doi: **http://doi:10.1130/b25770.1**

Placzek, C., Quade, J., Betancourt, J., Patchett, P., Rech, J., Latorre, C., Matmon, A., Holmgren, C., & English, N. (2009). Climate in the dry central Andes over geologic, millennial, and interannual timescale. Ann. Missouri Bot. Gard. 96, 386-397, doi: **http://doi:10.3417/2008019**

PMA (2007). Proyecto Multinacional Andino: Geociencia para las comunidades andinas. Movimientos en masa en la región andina, una guía para la evaluación de amenazas. Servicio Nacional de Geología y Minería. Publicación Multinacional No. 4, 432.

PMA (2008). Proyecto Multinacional Andino: Geociencia para las comunidades andinas. Experiencias andinas en mitigación de riesgos geológicos. Servicio Nacional de Geología y Minería. Publicación Geológica Multinacional No. 6, 106p

Pudasaini, S.P., & Krautblatter, M. (2022). The landslide velocity. Earth Surf. Dynam. 10, 165-189, doi: **https://doi.org/10.5194/esurf-10-165-2022.**

Reubi, O., & Hernandez, J. (2000). Volcanic debris avalanche deposits of the upper Maronne valley (Cantal Volcano, France): evidence for contrasted formation and transport mechanisms. J. Volcanol. Geoth. Res. 102, 271-286, doi: **https://doi.org/10.1016/S0377-0273(00)00191-8.**

Rodríguez, R. & Becerra, I. (2018). Arquitectura y evolución del Sistema de Fallas Incapuquio en el sector Palca-Tacna. Implicancia en la exploración de depósitos minerales. Boletin de la Sociedad Geológica del Perú. Publicación especial No. 14, 533-536. Resúmenes ampliados del XIX Congreso Peruano de Geología. www.sgp.org.pe ISSN 0079-1091.

Roperch, P., Sempere, T., Macedo, O., Arriagada, C., Fornari, M., Tapia, C., García, M., & Laj, C. (2006). Counterclockwise rotation of late Eocene-Oligocene fore-arc deposits in southern Peru and its significance for oroclinal bending in the central Andes. Tectonics, 25(3), 1-25.

Sánchez-Núñez, J.M., Gómez, J.C., Macías, J.L. & Arce, J.L. (2020). Pleistocene rock avalanche, damming, and secondary debris flow along the Cotahuasi river, Peru. J. South Am. Earth Sc. 104, 102901, doi: 10.1016/j.jsames.2020.102901

Schildgen, T., Balco, G., & Shuster, D. (2010). Canyon incision and knickpoint propagation recorded by apatite 4He/3He thermochronometry. Earth Plan. Sc. Lett. 293, 377-387, doi: **http://doi:10.1016/j.epsl.2010.03.009**

Scott, K.M., Vallance, J.W., Kerle, N., Macías, J.L., Strauch, W., & Devoli, G. (2005). Catastrophic precipitation-triggered lahar at Casita volcano, Nicaragua: occurrence, bulking and transformation. Earth Surf. Proc. Landf. 30, 59-79.

Sepúlveda, S.A., Rebolledo, S., McPhee, J., Lara, M., Cartes, M., Rubio, E., & Vásquez, J.P. (2014). Catastrophic, rainfall-induced debris flows in Andean villages of Tarapacá, Atacama Desert, northern Chile. Landslides, 11(3), 481-491.

Siebert, L. (2002). Landslide resulting from structural failure of volcanoes, in Evans, S.G. and DeGraff, J.V., eds., Catastrophic landslide: Effects, occurrence, and mechanisms: Boulder Colorado. Geol. Soc. Am. Rev. Eng. Geol. XV, 209-235

Steffen, D., Schlunegger, F., & Preusser, F. (2010). Late Pleitocene fans and terraces in the Majes valley, southern Peru, and their relation to climatic variations. Int. J Earth Sci (Geol Rundsch), 99, 1975-1989, doi: **http://doi:10.1016/10.1007/s00531-009-0489-2**

Stern, C.R. (2004). Active Andean volcanism: its geologic and tectonic setting. Andean Geol. Rev. Geológica de Chile, 31(2), 161-206

Strom, A.L., Li, L., & Lan, H. (2019). Rock avalanche mobility: optimal characterization and the effects of confinement. Landslide, 16, 1437-1452, doi: **http://doi:10.1016/10.1007/s10346-019-01181-z**

Sturm, S., Kenkmann, T., Willmes, M., Pösges, G., & Hiesinger, H. (2015). The distribution of megablocks in the Ries crater, Germany: Remote sensing, field investigation, and statistical analysis. Met. & Plan. Sc. 50(1), 141-171, doi: **http://doi:10.1016/10.1111/maps.12408**

Tapia-Baldis, C. T., Rothis, L. M., Perucca, L., Angillieri, M. E., Vargas, H., Ponce, D., & Allis, C. (2018). Analysis of La Dehesa paleolandslide. Central Pre-Andes of Argentina. J. South Amer. Earth. Sc. 83, 1-13. doi: **https://doi.org/10.1016/j.jsames.2018.01.011**

Tavera, H., Fernández, E., Salas, H., Antayhua, Y., Bernal, I. (2000). Mecanismo focal de los terremotos de Arequipa del 8 de octubre de 1998 (MW=6.0) y 3 de abril de 1999 (MW=6.5). Boletin de la Sociedad Geológica del Perú v. 89 p 21-31

Terrizzano, C.M., García Morabito, E., Christl, M., Likerman, J., Tobal, J., Yamin, M., & Zech, R. (2017). Climatic and tectonic forcing on alluvial fans in the southern central Andes. Quat. Sc. Rev. 172, 131-141, doi: **http://dx.doi.org/10.1016/j.quascirev.2017.08.002**

Thouret, J.C., Gunnell, Y., Jica, B.R., Paquette, J.L., & Braucher, R. (2017). Canyon incision chronology based on ignimbrite stratigraphy and cut-and-fill sediment sequences in SW Peru documents intermittent uplift of the western Central Andes. Geomorphology, 298, 1-19, doi: **http://doi.org/10.1016/j.geomorph.2017.09.013**

Thouret, J.C., Jica, B., Paquette, J.L., & Cubukcu, E. (2016). A 25 myr chronostratigraphy of ignimbrites in south Peru: implication for the volcanic history of the Central Andes. J. Geol. Soc. 173, 734-756.

Thouret, J.C., Wörner, G., Gunnell, Y., Singer, B., Zhang, X., & Souriot, T. (2007). Geochronologic and stratigraphic constraints on canyon incision and Miocene uplift of the Central Andes in Peru. Earth Planet. Sci. Lett. 263 (3-4), 151-166.

Tian, Y., Xu, C., Ma, S., Xu, X., Wang, S., Zhang, H. (2019). Inventory and spatial distribution of landslides triggered by the 8th August 2017 Mw 6.5 Jiuzhaigou earthquake, China. J. Earth Sc., 30, 206-217, doi: **https://doi.org/10.1007/s12583-018-0869-2.**

Wang, Y.F., Cheng, Q.G., & Zhu, Q. (2015). Facies succession of rock avalanches triggered by Wenchuan earthquake, Sichuan, China. In: Engineering geology for society and territory- Volume 2, Landslide pro-

cesses, Eds. Lollino G., Giordan D., Crosta G., Corominas J., Azzam R., Wasowski J., Sciarra N., Springer 2,177, doi: **http://doi:10.1007/978-3-319-09057-3**

Wang, Y.F., Dong, J.J., & Cheng, Q.G. (2017). Velocity-dependent frictional weaking of large rock avalanche basal facies: Implication for rock avalanche Hypermobility. J. Geophys. Res. Solid Earth, 122, 1648-1676, doi: **https://doi.org/10.1002/2016JB013624**

Weidinger, J., Korup, O., Munack, H., Altenberger, U., Dunning, S., Tippelt, G., & Lotteroser, W. (2014). Giant rockslides from the inside. Earth Plan. Sc. Lett. 389, 62-73, doi: **http://dx.doi.org/10.1016/j.epsl.2013.12.017**

Wilson, J., & García, W. (1962). Geología de los cuadrángulos de Pachia y Palca. Hojas 36-v y 36-x. Comisión de la Carta Geológica Nacional, p.85.

Witze, A. (2008). The volcano that changed the world. Nature, doi: **https://doi.org/10.1038/news.2008.747**

Zavala, B. (2017). Aspectos geológicos y geomorfológicos del valle y cañón Cotahuasi (Reserva paisajística Subcuenca de Cotahuasi, provincia La Unión, Arequipa). Instituto Geológico Mirero y Metalúrgico, INGEMMET, Lima, Perú. 10 p.